# EFFECT OF SOIL VARIABILITY ON THE BEARING CAPACITY OF FOOTINGS ON MULTI-LAYERED SOIL

By

Yien Lik Kuo

THESIS SUBMITTED FOR THE DEGREE OF

DOCTOR OF PHILOSOPHY (PHD)


SCHOOL OF CIVIL, ENVIRONMENTAL AND MINING

ENGINEERING

OCTOBER 2008

# CHAPTER 7

## ANN-BASED MODELS FOR PREDICTING BEARING CAPACITY ON A MULTI-LAYERED COHESIVE-FRICTIONAL SOIL PROFILE

# 7.1 INTRODUCTION

Traditionally, the ultimate bearing capacity, $Q_u$, of a shallow strip footing, which is founded on single-layered homogeneous cohesive-frictional, weightless deposit, in the absence of surcharge, can be expressed as:

$$Q_u = q_{u(c\text{-}\phi)} \times B \tag{7.1}$$

where $B$ is the width of the strip footing and $q_{u(c\text{-}\phi)}$ is the ultimate bearing pressure applied to the footing, and can be expressed as follows:

$$q_{u(c\text{-}\phi)} = c_u \times N_c \tag{7.2}$$

where $N_c$ is a non-dimensional bearing capacity factor, as previously mentioned. When considering the purely-cohesive and homogeneous case (i.e. $c \neq 0$, $\phi = 0$, where $\phi$ is the friction angle of soil), $N_c$ is equal to well-known Prantl solution of $(2+\pi)$. For a footing supported on a cohesive-frictional, homogeneous material, $N_c$ can be expressed as a function of $\phi$ and expressed as follows (Prandtl, 1921; Hill, 1950):

$$N_c = \frac{e^{\pi \tan\phi} \tan^2\left(\frac{\pi}{4} + \frac{\phi}{2}\right) - 1}{\tan\phi} \tag{7.3}$$

In reality, as discussed earlier, footings are most likely to be founded on multi-layered soils, in which the soil profile may consist of distinct layers having significantly different properties. Whilst rigorous solutions to the problem of strip footings founded on two-layered cohesive soils have been presented by several researchers, the determinination of the bearing capacity of footings on multi-layered, cohesive-frictional weightless soils remains empirical. Such an empirical method has been suggested by Bowles (1988) by adopting the weighted average soil strength, $c_{av}$ and $\phi_{av}$, of a number of cohesive-frictional layers as follows:

$$c_{av} = \frac{\sum_{i=1}^{n} c_i \, h_i}{\sum_{i=1}^{n} h_i} \tag{7.4}$$

$$\tan\phi_{av} = \frac{\sum_{i=1}^{n} (\tan\phi_i) \times h_i}{\sum_{i=1}^{n} h_i} \tag{7.5}$$

where $n$ is the total number of layers within the depth of soil which influences bearing capacity; $c_i$ and $\phi_i$ respectively represent the soil cohesion and friction angle; and, $h_i$ is the thickness of the $i$th stratum. This method was examined in the previous chapter and was shown to be unreliable for predicting the bearing capacity of footings founded on multi-layered, purely-cohesive soil. An ANN-based bearing capacity equation has been successfully developed in previous chapter for footings on purely-cohesive soils, and it was shown to be accurate and robust in predicting bearing capacities. Such an ANN-based model is expressed as function of the footing width, $B$, the stratum thickness, $h_i$, and the soil cohesion, $c_i$, as follows:

$$q_{u(c\text{-}\phi)} = f(c_i, h_i, B) \tag{7.6}$$

The main objective of this chapter is to develop a meta-model for predicting the bearing capacity of strip, rough footings supported on a ten-layered, cohesive-frictional, homogeneous and weightless material. In the next section, the details of two proposed methodologies are presented in order to achieve the objective stated above.

## 7.2 PROBLEM DEFINITION AND PROPOSED METHODOLOGIES

The problem considered in this chapter is illustrated in Figure 7.1. A rough, rigid strip footing of width, $B$, is founded on a ten-layered cohesive-frictional soil profile. The soil cohesion of each layer, $c_i$, is assumed to vary in the range between 1.0 and

10.0 kPa, whilst the friction angle of each layer, $\phi_i$, varies in between 5.0° and 20.0°. The footing width, $B$, will also be varied between 1.0 and 4.0 metres. The thickness of each soil layer, $h_i$, is not uniform but is varied from a minimum value of 0.2 to a maximum value of 1.0 metre.

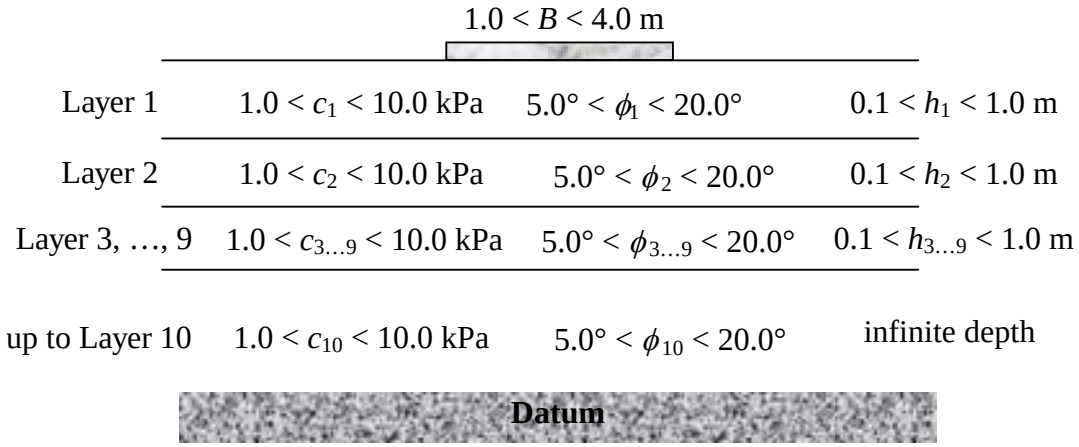


**Figure 7.1** Problem definition for 10-layered cohesive-frictional soil profile.

An ANN-based model for predicting the bearing capacity, $q_{u(c\text{-}\phi)}$, of cohesive-frictional soil layer will be developed and expressed using two different approaches. One will be expressed as a function of a number of variables, as follows:

$$q_{u(c\text{-}\phi)} = f(c_i,\ \phi_i,\ h_i,\ B) \tag{7.7}$$

Whilst, in another variation, $q_u$ is expressed in the following form:

$$q_{u\,(c-\phi)} = \tilde{N}_{c-\phi} \times \tilde{N}_c \times N_c \times c_1 \tag{7.8}$$

where $\tilde{N}_{c-\phi}$ and $\tilde{N}_c$ denote two newly introduced dimensionless factors, as explained below; $c_1$ is the soil cohesion of the uppermost layer, whilst, the friction angle of the uppermost soil layer, $\phi_1$, will be used to calculate the traditional bearing capacity dimensionless factor, $N_c$, as follows:

$$N_c = \frac{e^{\pi \tan \phi_1} \tan^2\left(\frac{\pi}{4} + \frac{\phi_1}{2}\right) - 1}{\tan \phi_1} \tag{7.9}$$

$\tilde{N}_c$ is a multi-layered factor for both purely-cohesive and cohesive-frictional soil layers and will be expressed in following form:

$$\tilde{N}_c = f(c_i, h_i, B) \tag{7.10}$$

$\tilde{N}_{c-\phi}$ is another multi-layered factor, which will have an assigned value of 1.0 for purely-cohesive case, and will be used in conjunction with $\tilde{N}_c$ to calculate the bearing capacity of a footing on cohesive-frictional multi-layered soil, and is defined as:

$$\tilde{N}_{c-\phi} = f(c_i, \phi_i, h_i, B) \tag{7.11}$$

In this study, ANN-based models will be developed for $q_{u(c)}$ and $q_{u(c\text{-}\phi)}$ in the form of a series of equations, as well as $\tilde{N}_c$ and $\tilde{N}_{c-\phi}$, obtained using Equations 7.10 and 7.11. In order to train the ANN models, data are required, and these can be obtained through a parametric study, as discussed below.

## 7.3 DATA GENERATION USING NUMERICAL FORMULATION OF LOWER BOUND THEOREM

Due to the large number of influencing factors, which include 10 cohesion values, 10 friction angles, 9 soil layer thicknesses, and the footing width, 5,000 Monte Carlo simulations are performed. As in previous chapter, finite element limit analysis is employed to perform the Monte Carlo simulations. However, in this study, only the lower bound finite element limit analysis will be used, as the lower bound computations give conservative estimates of the collapse load. Using the average of both the upper and lower bound computations, as in the previous chapter, may lead to an overestimate in the collapse load in some cases. When both upper and lower bound analyses were used, there is a need to employ a very fine mesh to reduce the

gap between the lower and upper bound solutions, which significantly compromise computational speed. In contrast, lower bound finite element analysis always gives estimates that are lower than the actual collapse load, regardless of any adopted finite element size.

For each realization, the values $c_i$, $\phi_i$ , $h_i$ and $B$ are randomly selected from a uniform distribution within predefined ranges, and later presented as inputs for the numerical simulations. The two-dimensional lower bound mesh for a strip footing founded on a 10-layered cohesive-frictional soil under plane strain conditions is shown in Figure 7.2. Due to the symmetric nature of the problem, the lower bound computation is carried out on half of the domain, as shown. The boundary conditions and the directions for the extension elements are also shown in Figure 7.2.

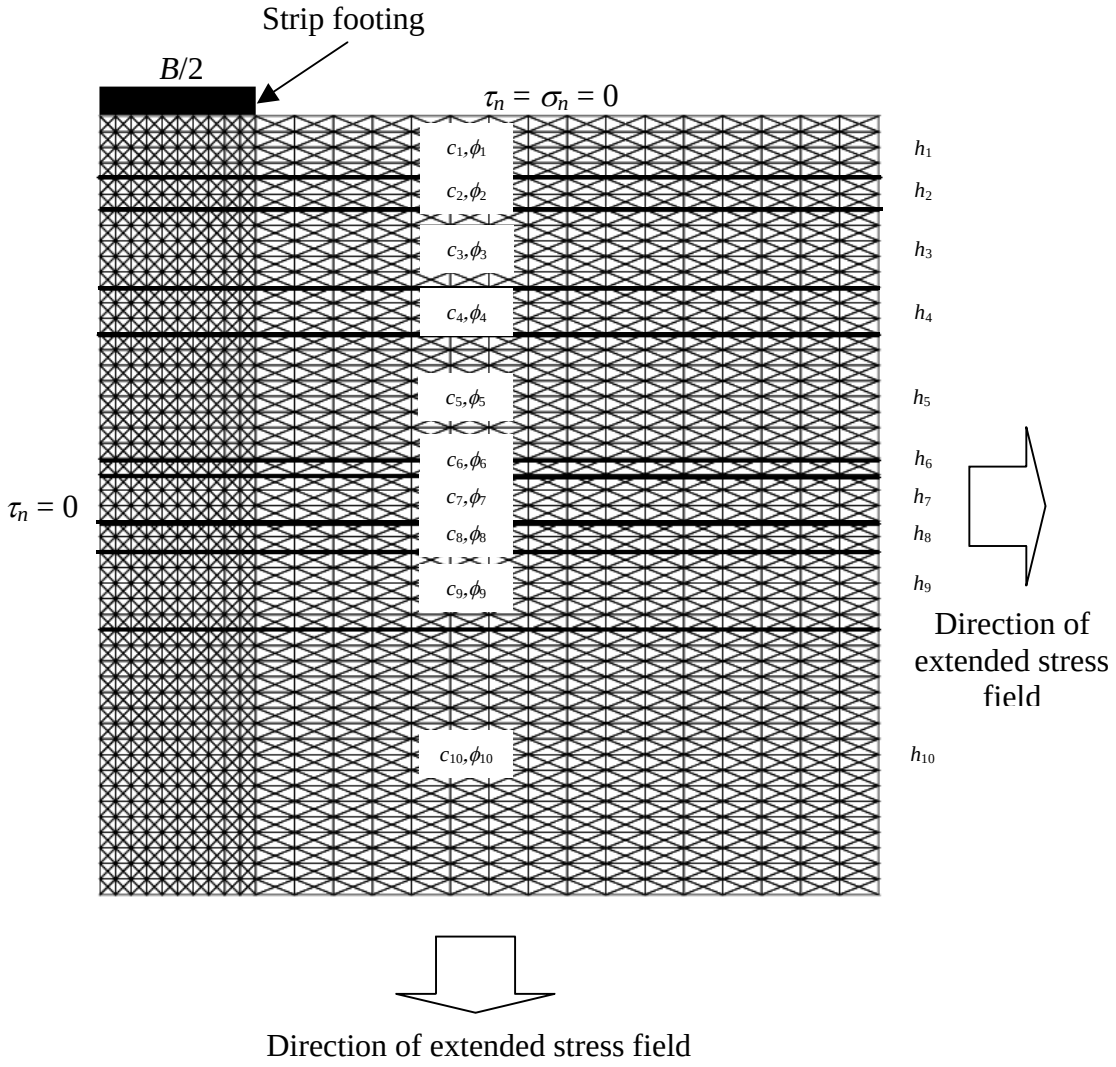


**Figure 7.2** Typical mesh for analysis of strip footing and directions of extensions for lower bound implementation.

In order to develop ANN-based models for $\tilde{N}_c$, and later for $\tilde{N}_{c-\phi}$, two separate numerical limit analyses are required for each realization: one for purely-cohesive cases, and another for cohesive-frictional cases. Different sets of influencing parameters are used for each case (i.e. {$c_i$, $h_i$, $B$} for purely-cohesive cases and {$c_i$, $\phi_i$, $h_i$, $B$} for cohesive-frictional cases). For purely-cohesive cases, the numerical limit analysis produces a bearing capacity, $q_{u(c)}$, which subsequently allows $\tilde{N}_c$ to be calculated. The value of $\tilde{N}_c$ will be used later together with $q_{u(c\text{-}\phi)}$ in determining $\tilde{N}_{c-\phi}$. Figure 7.3 illustrates the flow chart used in the proposed methodologies.

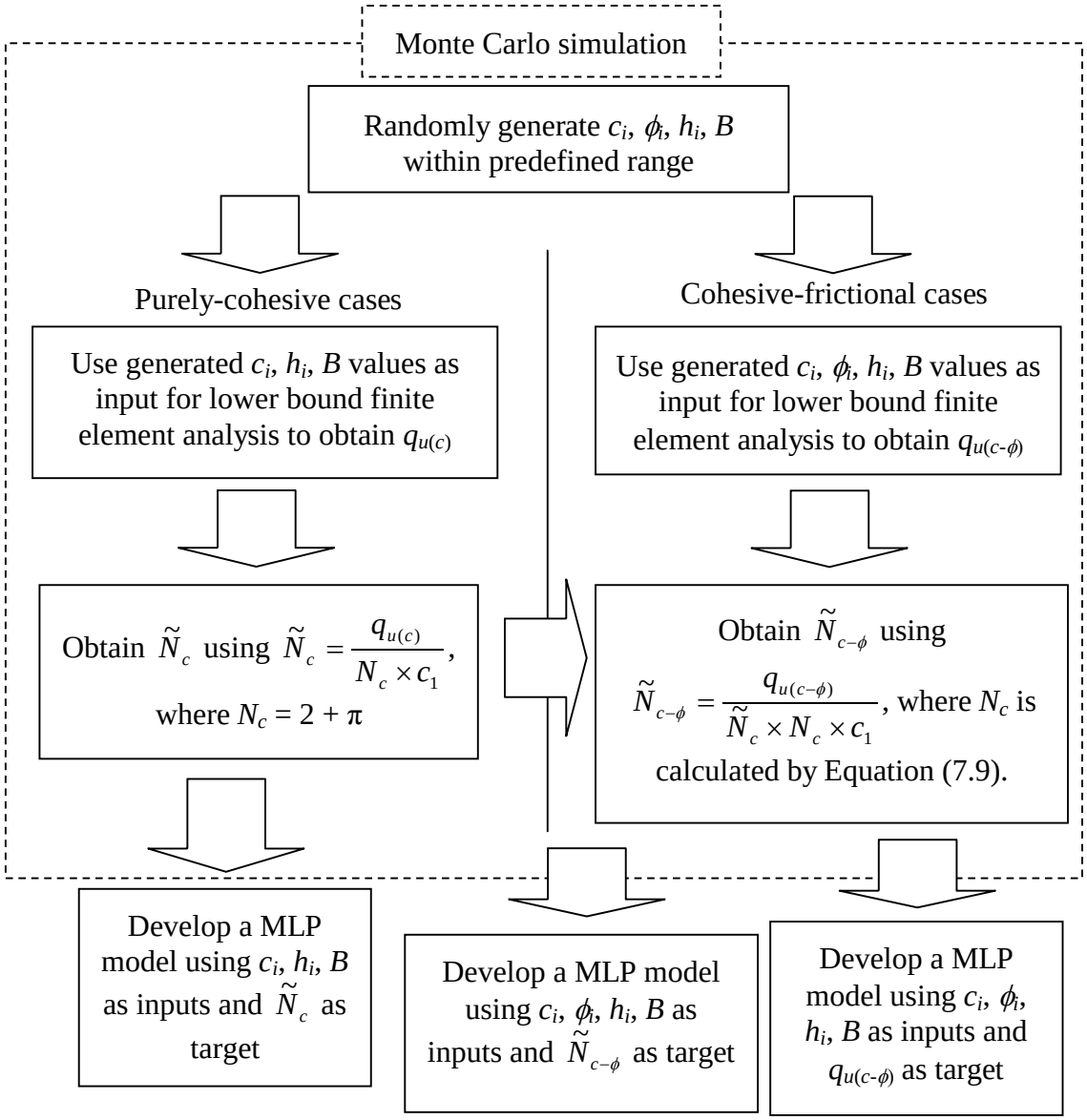


**Figure 7.3** Flow chart of the proposed methodologies.

## 7.4 DEVELOPMENT OF NEURAL NETWORK MODELS

In this study, the method of back-propagation multi-layer perceptrons (MLPs) in the *NEUFRAME* computer software (Neusciences, 2000) is employed to develop three separate MLP models for $q_{u(c\text{-}\phi)}$, $\tilde{N}_c$, and $\tilde{N}_{c-\phi}$, as shown previously in Figure 7.3. In total, 20 variables are presented to the MLP model as model inputs for $\tilde{N}_c$, whilst 30 are presented as model inputs for $\tilde{N}_c$ and $q_{u(c\text{-}\phi)}$. The data are divided into three sets, namely: training, testing and validation. When the data are divided into their subsets, it is required to check that the statistics of each of the training, testing and validation subsets represent the same population (Master, 1993). The basic standard statistics of the inputs and outputs are shown in Table C.1 in Appendix C, and the null hypothesis tests are carried out and summarised in Table C.2 in Appendix C. Cross validation is used as the stoping criteria. The momentum and the learning rates are set as the default values specified by *NEUFRAME* of 0.8 and 0.2, respectively.

In total, there are 4,000 data values, which account for 80% of the total available data, are used for training purposes and the remaining 1,000 data or 20% are used for validation. For those 4,000 data used for training, these are further divided into 70% (i.e. 2,800) for training and 30% (i.e. 1,200) for the testing sets. As in previous chapter, data division is achieved by using random selection, and *t*-test and *F*-test were carried out to ensure that the statistic properties between three data sets are consistent. The results of *t*-test and *F*-test are presented in Appendix C.

After the data division process, all variables were scaled between 0 and 1 by using simple linear mapping of the variables' practical extreme to the neural networks' extreme, using $x_n = (x - x_{\min})/(x_{\max} - x_{\min})$, where $x_n$ is the scaled value, $x$ is the relevant variable, and $x_{\min}$ and $x_{\max}$ are the minimum and maximum values, respectively. This pre-processing ensures that all variables receive equal attention during the training process.

Training is carried out using one hidden layer, with a minimum of 1 up to $2I+1$ hidden nodes, where $I$ is the number of input variables, for each MLP model. A network with

one hidden layer is suggested to be sufficient for mapping any continuous function (Cybenko, 1989; Hornik et al., 1989). It is suggested that $2I+1$ is the upper limit of the number of hidden nodes (Caudill, 1988). The performance of the networks is measured by coefficient of correlation, *r*, root mean square error, RMSE, and mean absolute error, MAE. The strategy adopted in this study for accessing the optimum MLP model is that a model is deemed to be optimal if it satisfies three requirements: the model performs well with respect to the testing set; it has a minimum number of hidden nodes; and it has consistent performance with the validation set as with that obtained from the training and testing sets.

The results of the networks' performance for each of the models, with respect to number of hidden layer nodes, are summarised in Tables 7.1, 7.2 and 7.3, and also illustrated graphically in Figures 7.4, 7.5 and 7.6. The results show that the number of hidden layer nodes has a significant effect on the models' performance. The networks with less than 5 nodes are among the lowest in terms of *r* values and the highest with respect to RMSE and MAE values, which indicated unsatisfactory performance and an unacceptably large predictive error. It can be seen from the results that, in general, the predictive error reduces with increasing number of hidden layer nodes. For all three models, the *r*, RMSE and MAE stabilise after the number of hidden layers nodes is equal to and larger than nine (as highlighted in Tables 7.1, 7.2 and 7.3). In the interests of developing a parsimonious model, a network with 9 hidden layer nodes is selected for $q_{u(c\text{-}\phi)}$, and coincidently, networks with same number of hidden layer nodes are selected for $\tilde{N}_c$ and $\tilde{N}_{c-\phi}$. The optimum structures of the MLP models are illustrated in Figures 7.7, 7.8 and 7.9.

## 7.5 BEARING CAPACITY EQUATION

The developed MLP models are then translated into relatively simple equations, based on the results from the *NEUFRAME* software and the optimal structure of MLP, which are suitable for hand calculations. Note that both the input and output have been rescaled, therefore, actual values for the input variables can be used in order to obtain the actual value of the bearing capacity. With reference to Figure 7.7, and the optimal MLP model, $q_{u(c\text{-}\phi)}$, is expressed as follows:

**Table 7.1** Performance results of ANN models for $q_{u(c\text{-}\phi)}$.

| Model number | No. hidden layer nodes | Data sets | | | | | | | | |
|---|---|---|---|---|---|---|---|---|---|---|
| | | Training set | | | Testing set | | | Validation set | | |
| | | Performance measures | | | | | | | | |
| | | $r$ | RMSE (kN/m$^2$) | MAE (kN/m$^2$) | $r$ | RMSE (kN/m$^2$) | MAE (kN/m$^2$) | $r$ | RMSE (kN/m$^2$) | MAE (kN/m$^2$) |
| Qu_1 | 1 | 0.817 | 9.003 | 7.266 | 0.828 | 9.028 | 7.333 | 0.825 | 9.163 | 7.518 |
| Qu_3 | 3 | 0.923 | 5.794 | 4.450 | 0.924 | 5.779 | 4.450 | 0.920 | 5.881 | 4.526 |
| Qu_5 | 5 | 0.942 | 4.793 | 3.677 | 0.940 | 4.965 | 3.843 | 0.936 | 5.102 | 3.913 |
| Qu_7 | 7 | 0.957 | 4.325 | 3.370 | 0.950 | 4.645 | 3.625 | 0.945 | 4.792 | 3.745 |
| **Qu_9** | **9** | **0.963** | **3.976** | **3.084** | **0.957** | **4.332** | **3.374** | **0.953** | **4.571** | **3.608** |
| Qu_11 | 11 | 0.967 | 3.681 | 2.859 | 0.959 | 4.163 | 3.249 | 0.956 | 4.355 | 3.390 |
| Qu_13 | 13 | 0.963 | 3.898 | 3.042 | 0.951 | 4.529 | 3.526 | 0.948 | 4.674 | 3.660 |
| Qu_15 | 15 | 0.967 | 3.734 | 2.929 | 0.960 | 4.165 | 3.245 | 0.957 | 4.373 | 3.377 |
| Qu_17 | 17 | 0.966 | 3.871 | 3.026 | 0.958 | 4.336 | 3.413 | 0.956 | 4.494 | 3.515 |
| Qu_19 | 19 | 0.976 | 3.158 | 2.452 | 0.966 | 3.792 | 2.963 | 0.963 | 3.906 | 3.018 |
| Qu_21 | 21 | 0.968 | 3.661 | 2.859 | 0.959 | 4.183 | 3.269 | 0.958 | 4.308 | 3.346 |
| Qu_23 | 23 | 0.971 | 3.556 | 2.793 | 0.957 | 4.310 | 3.358 | 0.957 | 4.351 | 3.385 |
| Qu_25 | 25 | 0.975 | 3.202 | 2.496 | 0.962 | 3.996 | 3.124 | 0.960 | 4.135 | 3.202 |
| Qu_27 | 27 | 0.970 | 3.529 | 2.748 | 0.960 | 4.105 | 3.207 | 0.959 | 4.182 | 3.259 |
| Qu_29 | 29 | 0.969 | 3.633 | 2.831 | 0.959 | 4.212 | 3.311 | 0.958 | 4.268 | 3.342 |
| Qu_31 | 31 | 0.979 | 3.004 | 2.355 | 0.965 | 3.855 | 3.016 | 0.963 | 4.020 | 3.152 |
| Qu_33 | 33 | 0.972 | 3.420 | 2.664 | 0.960 | 4.105 | 3.226 | 0.960 | 4.141 | 3.225 |
| Qu_35 | 35 | 0.975 | 3.207 | 2.505 | 0.962 | 3.956 | 3.107 | 0.961 | 4.049 | 3.148 |
| Qu_37 | 37 | 0.974 | 3.321 | 2.605 | 0.961 | 4.078 | 3.179 | 0.962 | 4.075 | 3.207 |
| Qu_39 | 39 | 0.978 | 3.082 | 2.422 | 0.964 | 3.892 | 3.039 | 0.964 | 3.941 | 3.061 |
| Qu_41 | 41 | 0.971 | 3.427 | 2.684 | 0.959 | 4.134 | 3.215 | 0.957 | 4.204 | 3.263 |
| Qu_43 | 43 | 0.977 | 3.107 | 2.441 | 0.963 | 3.957 | 3.120 | 0.964 | 3.946 | 3.095 |
| Qu_45 | 45 | 0.975 | 3.238 | 2.530 | 0.964 | 3.897 | 3.024 | 0.961 | 4.090 | 3.165 |
| Qu_47 | 47 | 0.979 | 2.921 | 2.298 | 0.964 | 3.897 | 3.071 | 0.962 | 4.013 | 3.147 |
| Qu_49 | 49 | 0.978 | 3.130 | 2.446 | 0.964 | 3.973 | 3.105 | 0.961 | 4.083 | 3.143 |
| Qu_51 | 51 | 0.972 | 3.422 | 2.680 | 0.957 | 4.228 | 3.320 | 0.958 | 4.198 | 3.275 |
| Qu_53 | 53 | 0.980 | 2.872 | 2.253 | 0.966 | 3.820 | 2.984 | 0.963 | 3.921 | 3.055 |
| Qu_55 | 55 | 0.981 | 2.775 | 2.191 | 0.966 | 3.793 | 3.001 | 0.964 | 3.887 | 3.060 |
| Qu_57 | 57 | 0.975 | 3.239 | 2.543 | 0.963 | 3.972 | 3.085 | 0.959 | 4.118 | 3.209 |
| Qu_59 | 59 | 0.971 | 3.539 | 2.786 | 0.959 | 4.204 | 3.299 | 0.958 | 4.323 | 3.380 |
| Qu_61 | 61 | 0.977 | 3.090 | 2.421 | 0.964 | 3.899 | 3.046 | 0.962 | 3.948 | 3.068 |

**Table 7.2** Performance results of ANN models for $\tilde{N}_c$.

| Model number | No. hidden layer nodes | Data sets | | | | | | | | |
|---|---|---|---|---|---|---|---|---|---|---|
| | | Training set | | | Testing set | | | Validation set | | |
| | | Performance measures | | | | | | | | |
| | | *r* | RMSE ($kN/m^2$) | MAE ($kN/m^2$) | *r* | RMSE ($kN/m^2$) | MAE ($kN/m^2$) | *r* | RMSE ($kN/m^2$) | MAE ($kN/m^2$) |
| NC_1 | 1 | 0.839 | 0.172 | 0.125 | 0.840 | 0.162 | 0.121 | 0.846 | 0.159 | 0.119 |
| NC_3 | 3 | 0.932 | 0.114 | 0.087 | 0.920 | 0.117 | 0.089 | 0.925 | 0.113 | 0.085 |
| NC_5 | 5 | 0.968 | 0.080 | 0.061 | 0.960 | 0.084 | 0.064 | 0.962 | 0.083 | 0.063 |
| NC_7 | 7 | 0.964 | 0.085 | 0.066 | 0.955 | 0.089 | 0.067 | 0.959 | 0.086 | 0.066 |
| **NC_9** | **9** | **0.978** | **0.065** | **0.050** | **0.970** | **0.073** | **0.054** | **0.971** | **0.072** | **0.054** |
| NC_11 | 11 | 0.979 | 0.065 | 0.049 | 0.973 | 0.069 | 0.052 | 0.974 | 0.069 | 0.052 |
| NC_13 | 13 | 0.980 | 0.063 | 0.048 | 0.974 | 0.068 | 0.049 | 0.975 | 0.067 | 0.051 |
| NC_15 | 15 | 0.981 | 0.061 | 0.047 | 0.972 | 0.071 | 0.052 | 0.973 | 0.070 | 0.052 |
| NC_17 | 17 | 0.986 | 0.054 | 0.042 | 0.979 | 0.061 | 0.045 | 0.980 | 0.061 | 0.046 |
| NC_19 | 19 | 0.984 | 0.058 | 0.045 | 0.974 | 0.068 | 0.050 | 0.975 | 0.069 | 0.051 |
| NC_21 | 21 | 0.985 | 0.056 | 0.043 | 0.975 | 0.067 | 0.049 | 0.977 | 0.065 | 0.049 |
| NC_23 | 23 | 0.986 | 0.054 | 0.042 | 0.978 | 0.063 | 0.047 | 0.977 | 0.067 | 0.050 |
| NC_25 | 25 | 0.987 | 0.051 | 0.039 | 0.976 | 0.065 | 0.048 | 0.977 | 0.065 | 0.049 |
| NC_27 | 27 | 0.987 | 0.052 | 0.040 | 0.975 | 0.067 | 0.049 | 0.975 | 0.068 | 0.051 |
| NC_29 | 29 | 0.987 | 0.051 | 0.040 | 0.977 | 0.063 | 0.047 | 0.979 | 0.063 | 0.048 |
| NC_31 | 31 | 0.987 | 0.053 | 0.041 | 0.974 | 0.069 | 0.050 | 0.977 | 0.067 | 0.051 |
| NC_33 | 33 | 0.988 | 0.050 | 0.039 | 0.977 | 0.064 | 0.047 | 0.978 | 0.065 | 0.049 |
| NC_35 | 35 | 0.984 | 0.058 | 0.045 | 0.974 | 0.068 | 0.050 | 0.975 | 0.068 | 0.051 |
| NC_37 | 37 | 0.988 | 0.051 | 0.040 | 0.976 | 0.065 | 0.049 | 0.975 | 0.068 | 0.051 |
| NC_39 | 39 | 0.987 | 0.052 | 0.040 | 0.977 | 0.065 | 0.048 | 0.978 | 0.066 | 0.049 |
| NC_41 | 41 | 0.991 | 0.044 | 0.034 | 0.978 | 0.062 | 0.045 | 0.977 | 0.066 | 0.050 |

**Table 7.3** Performance results of ANN models for $\tilde{N}_{c-\phi}$.

| Model number | No. hidden layer nodes | Data sets | | | | | | | | |
|---|---|---|---|---|---|---|---|---|---|---|
| | | Training set | | | Testing set | | | Validation set | | |
| | | Performance measures | | | | | | | | |
| | | $r$ | RMSE (kN/m$^2$) | MAE (kN/m$^2$) | $r$ | RMSE (kN/m$^2$) | MAE (kN/m$^2$) | $r$ | RMSE (kN/m$^2$) | MAE (kN/m$^2$) |
| NF_1 | 1 | 0.734 | 0.177 | 0.134 | 0.738 | 0.169 | 0.130 | 0.721 | 0.174 | 0.130 |
| NF_3 | 3 | 0.858 | 0.131 | 0.097 | 0.850 | 0.128 | 0.097 | 0.838 | 0.134 | 0.099 |
| NF_5 | 5 | 0.869 | 0.125 | 0.089 | 0.867 | 0.119 | 0.088 | 0.849 | 0.130 | 0.093 |
| NF_7 | 7 | 0.895 | 0.118 | 0.089 | 0.884 | 0.119 | 0.091 | 0.874 | 0.124 | 0.093 |
| **NF_9** | **9** | **0.902** | **0.112** | **0.082** | **0.890** | **0.112** | **0.084** | **0.877** | **0.121** | **0.089** |
| NF_11 | 11 | 0.918 | 0.106 | 0.083 | 0.889 | 0.117 | 0.090 | 0.876 | 0.123 | 0.091 |
| NF_13 | 13 | 0.919 | 0.099 | 0.074 | 0.895 | 0.106 | 0.079 | 0.886 | 0.112 | 0.081 |
| NF_15 | 15 | 0.927 | 0.097 | 0.074 | 0.892 | 0.110 | 0.084 | 0.887 | 0.114 | 0.084 |
| NF_17 | 17 | 0.917 | 0.099 | 0.075 | 0.884 | 0.111 | 0.083 | 0.878 | 0.116 | 0.084 |
| NF_19 | 19 | 0.924 | 0.096 | 0.073 | 0.885 | 0.111 | 0.083 | 0.883 | 0.114 | 0.082 |
| NF_21 | 21 | 0.925 | 0.095 | 0.071 | 0.888 | 0.109 | 0.082 | 0.876 | 0.117 | 0.085 |
| NF_23 | 23 | 0.936 | 0.089 | 0.068 | 0.892 | 0.109 | 0.081 | 0.875 | 0.119 | 0.087 |
| NF_25 | 25 | 0.938 | 0.087 | 0.066 | 0.894 | 0.107 | 0.079 | 0.886 | 0.113 | 0.083 |
| NF_27 | 27 | 0.939 | 0.087 | 0.066 | 0.889 | 0.110 | 0.081 | 0.886 | 0.113 | 0.083 |
| NF_29 | 29 | 0.932 | 0.090 | 0.068 | 0.886 | 0.110 | 0.081 | 0.883 | 0.114 | 0.081 |
| NF_31 | 31 | 0.938 | 0.086 | 0.066 | 0.888 | 0.109 | 0.080 | 0.884 | 0.114 | 0.083 |
| NF_33 | 33 | 0.939 | 0.087 | 0.066 | 0.891 | 0.109 | 0.081 | 0.881 | 0.116 | 0.085 |
| NF_35 | 35 | 0.946 | 0.084 | 0.065 | 0.890 | 0.112 | 0.083 | 0.885 | 0.116 | 0.085 |
| NF_37 | 37 | 0.950 | 0.078 | 0.060 | 0.889 | 0.109 | 0.080 | 0.887 | 0.113 | 0.081 |
| NF_39 | 39 | 0.950 | 0.078 | 0.060 | 0.889 | 0.109 | 0.080 | 0.887 | 0.113 | 0.081 |
| NF_41 | 41 | 0.942 | 0.084 | 0.064 | 0.891 | 0.108 | 0.080 | 0.883 | 0.114 | 0.081 |
| NF_43 | 43 | 0.937 | 0.087 | 0.066 | 0.886 | 0.110 | 0.081 | 0.880 | 0.116 | 0.084 |
| NF_45 | 45 | 0.948 | 0.086 | 0.065 | 0.897 | 0.110 | 0.081 | 0.882 | 0.119 | 0.086 |
| NF_47 | 47 | 0.939 | 0.086 | 0.065 | 0.889 | 0.109 | 0.081 | 0.884 | 0.114 | 0.082 |
| NF_49 | 49 | 0.939 | 0.086 | 0.065 | 0.892 | 0.107 | 0.080 | 0.880 | 0.116 | 0.084 |
| NF_51 | 51 | 0.947 | 0.081 | 0.062 | 0.892 | 0.108 | 0.080 | 0.888 | 0.112 | 0.082 |
| NF_53 | 53 | 0.948 | 0.086 | 0.065 | 0.891 | 0.114 | 0.086 | 0.877 | 0.122 | 0.089 |
| NF_55 | 55 | 0.942 | 0.084 | 0.064 | 0.885 | 0.111 | 0.083 | 0.880 | 0.115 | 0.084 |
| NF_57 | 57 | 0.942 | 0.084 | 0.064 | 0.891 | 0.109 | 0.080 | 0.882 | 0.115 | 0.083 |
| NF_59 | 59 | 0.950 | 0.085 | 0.064 | 0.897 | 0.110 | 0.082 | 0.885 | 0.119 | 0.087 |
| NF_61 | 61 | 0.951 | 0.077 | 0.060 | 0.872 | 0.118 | 0.088 | 0.872 | 0.120 | 0.088 |

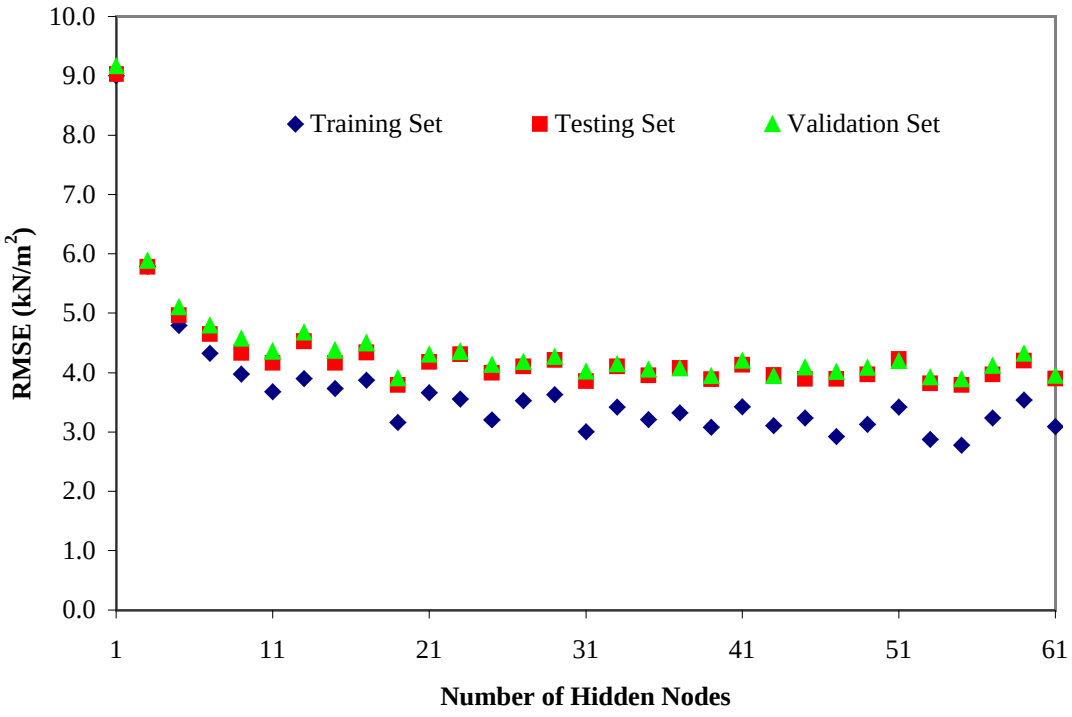


**Figure 7.4** Root mean square error versus number of hidden layer nodes for $q_{u(c\text{-}\phi)}$.

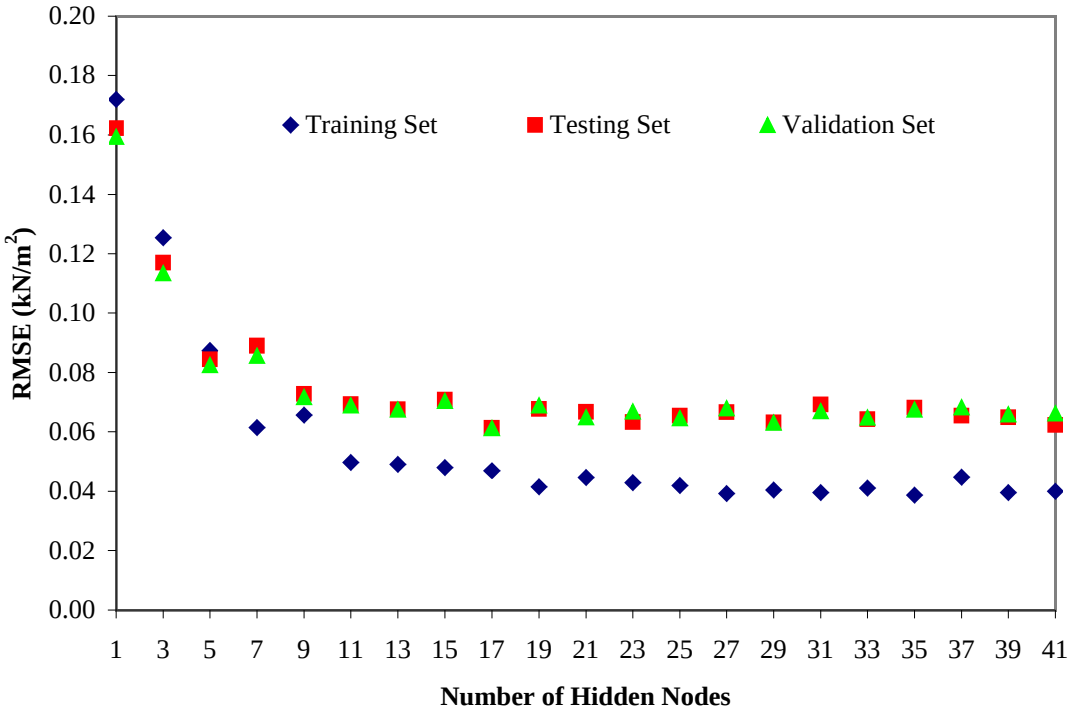


**Figure 7.5** Root mean square error versus number of hidden layer nodes for $\tilde{N}_c$.

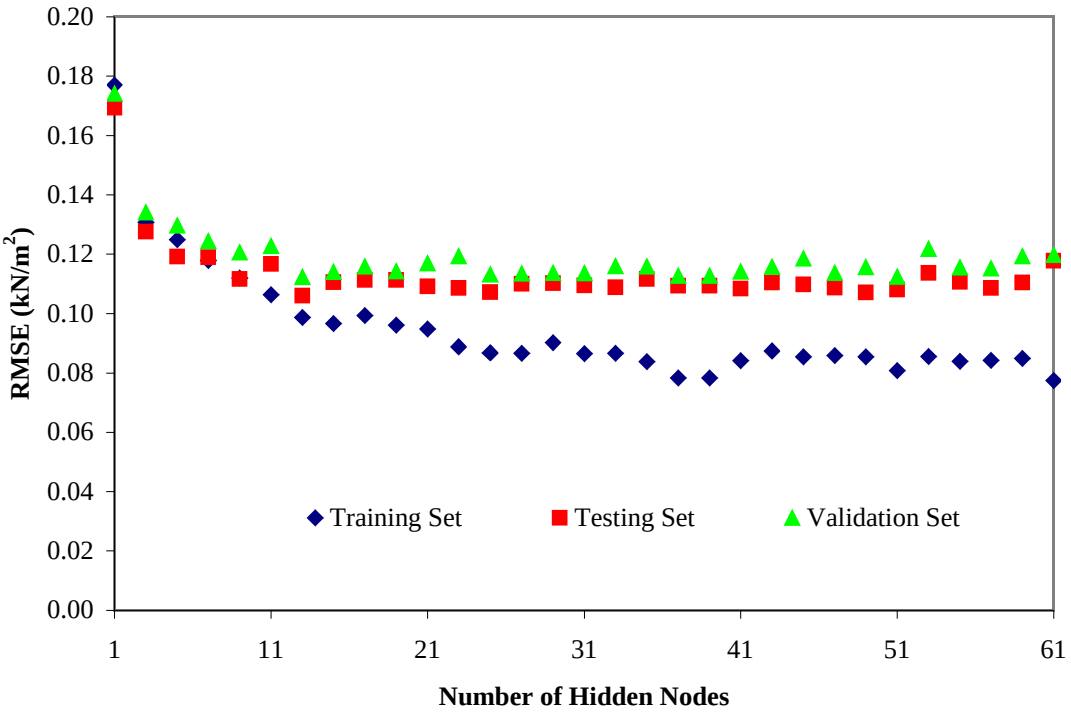


**Figure 7.6** Root mean square error versus number of hidden layer nodes for $\tilde{N}_{c-\phi}$.

$$q_{u(c-\phi)} = \left[ \frac{86.065}{1+\exp\left( \begin{array}{l} 4.239T_1 - 3.821T_2 + 4.867T_3 - 2.804T_4 \\ -2.709T_5 - 2.597T_6 - 3.746T_7 + 3.475T_8 \\ +3.613T_9 + 4.080 \end{array} \right)} + 7.245 \right] \tag{7.12}$$

where $T_{i=1,\ldots 9}$ represent the hidden layer nodes as shown in Figure 7.7, which are calculated as:

$$T_{i=1,\ldots,9} = \left[ 1+\exp\left( \begin{array}{l} w_1 c_1 + w_2 c_2 + w_3 c_3 + w_4 c_4 + w_5 c_5 + w_6 c_6 \\ + w_7 c_7 + w_8 c_8 + w_9 c_9 + w_{10} c_{10} + w_{11} \phi_1 \\ + w_{12} \phi_2 + w_{13} \phi_3 + w_{14} \phi_4 + w_{15} \phi_5 + w_{16} \phi_6 \\ + w_{17} \phi_7 + w_{18} \phi_8 + w_{19} \phi_9 + w_{20} \phi_{10} + w_{21} h_1 \\ + w_{22} h_2 + w_{23} h_3 + w_{24} h_4 + w_{25} h_5 + w_{26} h_6 \\ + w_{27} h_7 + w_{28} h_8 + w_{29} h_9 + w_{30} B + C \end{array} \right) \right]^{-1} \tag{7.13}$$

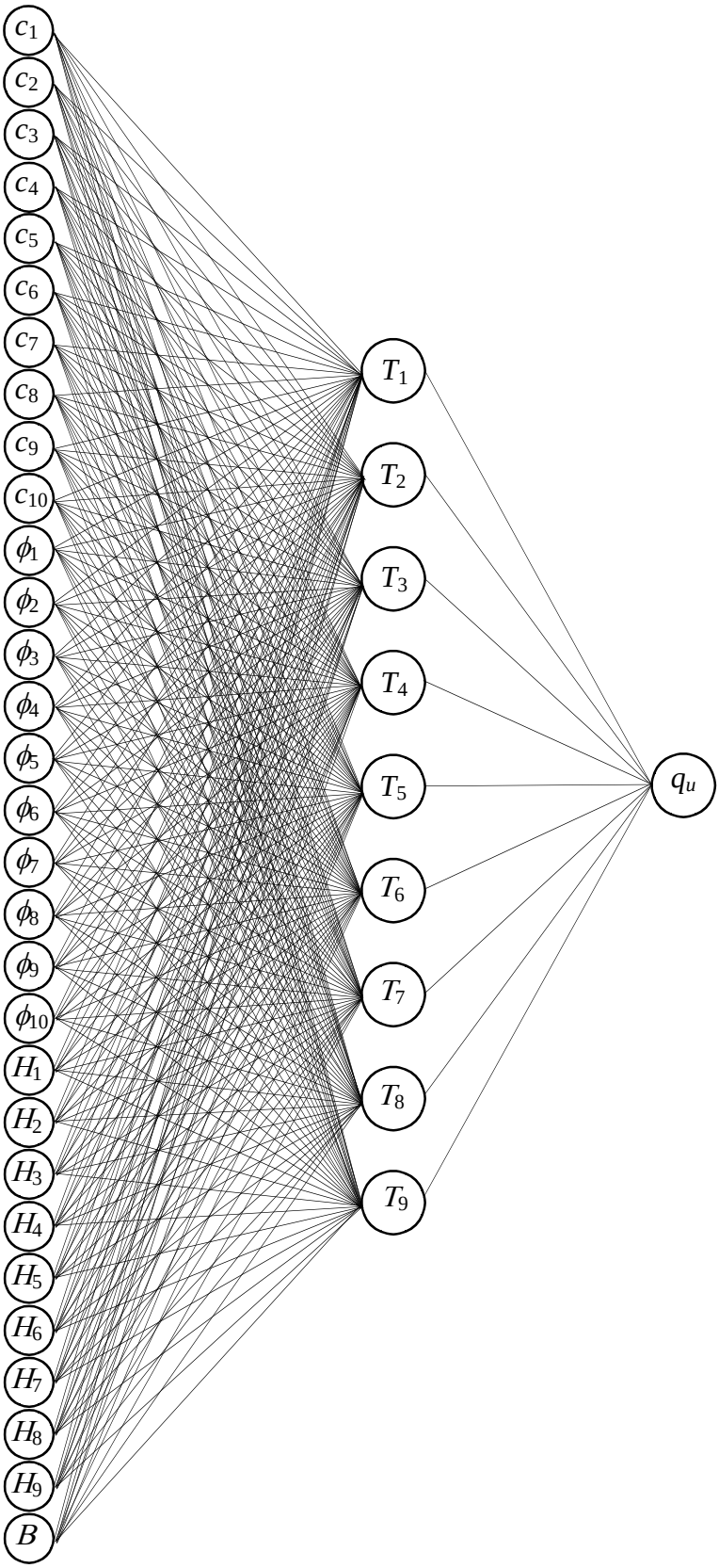


**Figure 7.7** Structure of optimum MLP model for $q_{u(c\text{-}\phi)}$.

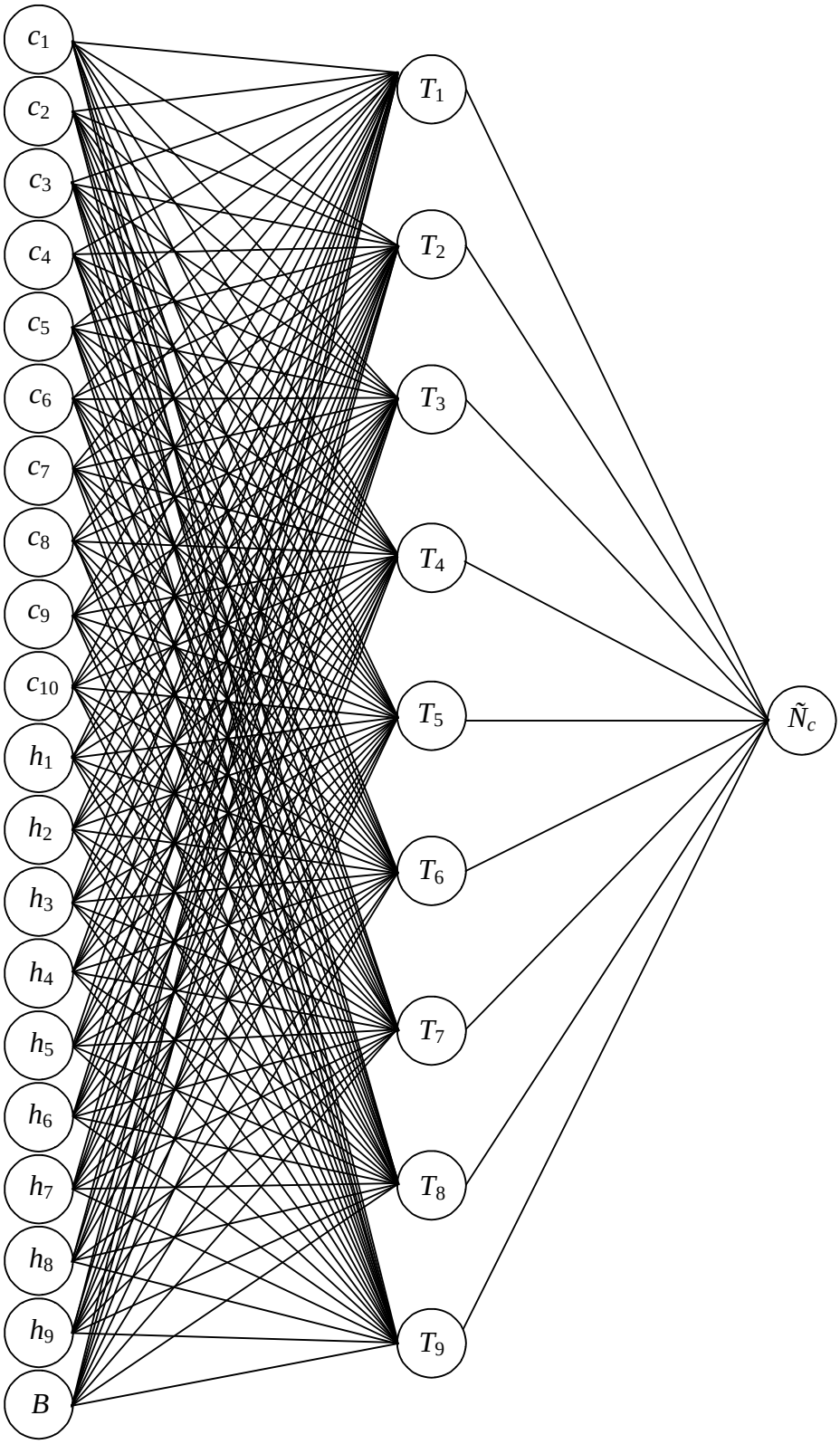


**Figure 7.8** Structure of optimum MLP model for $\tilde{N}_c$.

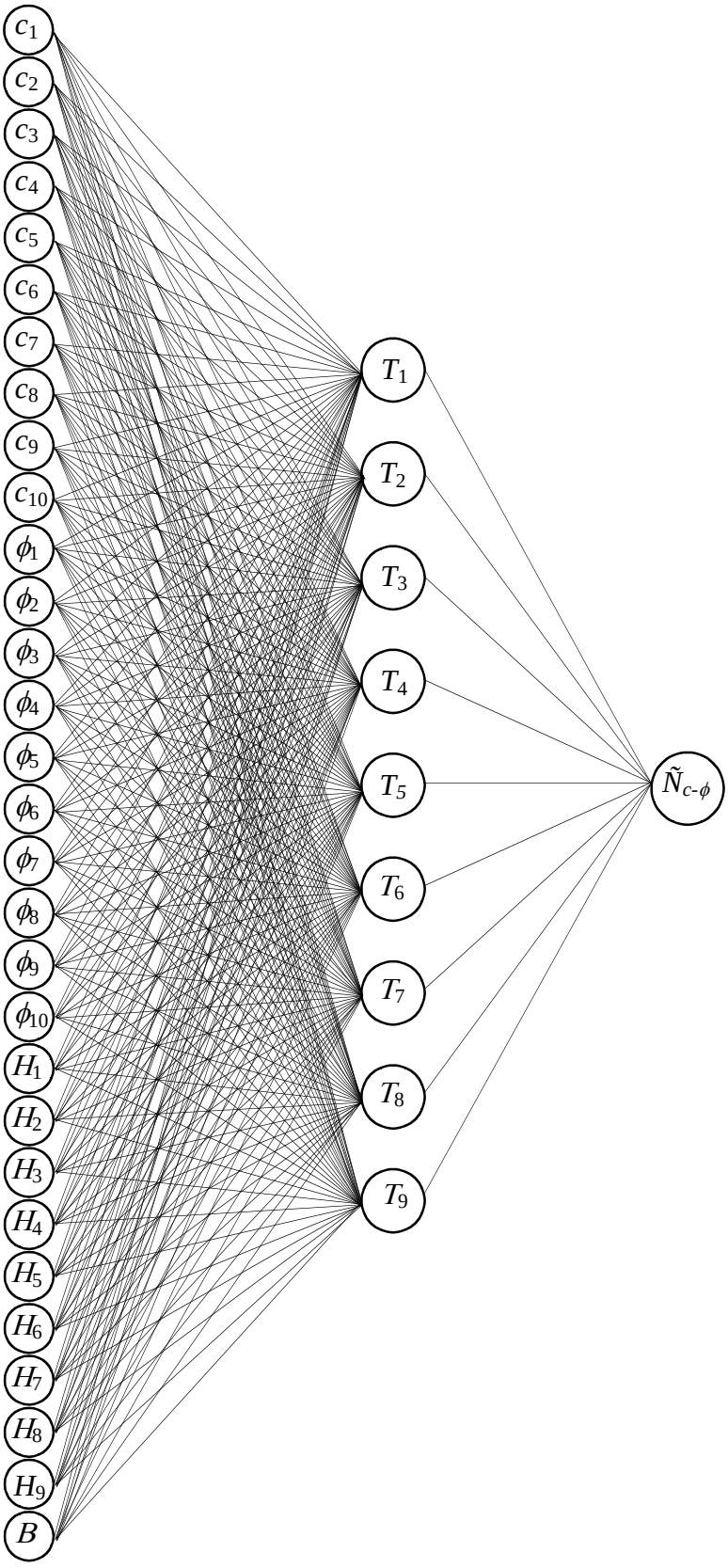


**Figure 7.9** Structure of optimum MLP model for $\tilde{N}_{c\text{-}\phi}$.

**Table 7.4** Value of $w_{i=1,\ldots,30}$ and $C$ versus $T_{i=1,\ldots,9}$ for $q_{u(c\text{-}\phi)}$

| | $T_1$ | $T_2$ | $T_3$ | $T_4$ | $T_5$ | $T_6$ | $T_7$ | $T_8$ | $T_9$ |
|---|---|---|---|---|---|---|---|---|---|
| $w_1$ | -0.409 | -0.404 | 0.205 | -0.061 | -0.109 | -0.072 | -0.057 | -0.155 | 0.061 |
| $w_2$ | 0.176 | -0.116 | -0.189 | 0.037 | -0.012 | -0.047 | 0.068 | 0.331 | -0.004 |
| $w_3$ | 0.081 | 0.140 | 0.134 | -0.053 | -0.008 | -0.120 | 0.221 | 0.112 | -0.020 |
| $w_4$ | 0.054 | 0.054 | -0.002 | -0.128 | 0.275 | -0.115 | -0.073 | 0.001 | -0.022 |
| $w_5$ | 0.034 | 0.058 | -0.084 | -0.130 | -0.096 | 0.005 | -0.018 | -0.073 | -0.029 |
| $w_6$ | 0.014 | 0.073 | 0.009 | 0.026 | -0.059 | 0.055 | -0.080 | 0.006 | -0.037 |
| $w_7$ | 0.004 | 0.044 | 0.029 | -0.013 | -0.023 | 0.080 | -0.050 | 0.028 | -0.036 |
| $w_8$ | 0.001 | 0.021 | 0.004 | 0.009 | -0.017 | -0.001 | -0.015 | 0.004 | -0.009 |
| $w_9$ | -0.002 | 0.006 | 0.015 | -0.003 | -0.008 | 0.047 | -0.022 | 0.026 | -0.025 |
| $w_{10}$ | 0.006 | 0.013 | 0.013 | 0.029 | 0.002 | 0.013 | -0.019 | 0.002 | 0.005 |
| $w_{11}$ | -0.071 | -0.063 | 0.035 | 0.007 | -0.041 | -0.008 | -0.028 | -0.052 | 0.040 |
| $w_{12}$ | 0.047 | -0.011 | -0.037 | 0.063 | -0.007 | -0.042 | -0.006 | 0.055 | -0.003 |
| $w_{13}$ | 0.022 | 0.037 | 0.021 | 0.005 | -0.001 | -0.067 | 0.051 | 0.005 | -0.004 |
| $w_{14}$ | 0.004 | 0.009 | -0.010 | -0.045 | 0.047 | -0.023 | -0.020 | 0.001 | -0.016 |
| $w_{15}$ | -0.001 | 0.014 | -0.020 | -0.031 | -0.035 | -0.015 | 0.006 | -0.028 | 0.001 |
| $w_{16}$ | -0.004 | 0.011 | -0.004 | 0.024 | -0.032 | 0.001 | -0.019 | -0.003 | -0.005 |
| $w_{17}$ | 0.001 | 0.014 | 0.012 | 0.004 | -0.008 | 0.037 | -0.020 | 0.018 | -0.004 |
| $w_{18}$ | -0.006 | 0.000 | -0.001 | 0.002 | -0.002 | -0.015 | 0.002 | -0.002 | -0.002 |
| $w_{19}$ | 0.001 | -0.001 | -0.003 | 0.004 | 0.006 | 0.001 | -0.007 | 0.006 | 0.003 |
| $w_{20}$ | -0.002 | 0.009 | 0.005 | 0.002 | 0.002 | 0.010 | -0.012 | 0.012 | -0.002 |
| $w_{21}$ | 1.202 | 1.660 | -0.794 | -0.116 | 0.339 | -0.176 | 0.410 | 1.287 | 1.666 |
| $w_{22}$ | 0.427 | 1.079 | 0.778 | -0.535 | 0.291 | 0.840 | -0.116 | -0.999 | 0.391 |
| $w_{23}$ | 0.101 | -0.101 | -0.620 | -0.200 | 0.313 | 0.926 | -1.402 | -0.216 | 0.118 |
| $w_{24}$ | -0.202 | 0.230 | -0.004 | 0.220 | -1.571 | 0.992 | -0.206 | 0.009 | -0.029 |
| $w_{25}$ | 0.020 | 0.143 | 0.434 | 0.553 | 0.395 | 0.452 | -0.544 | 0.320 | -0.143 |
| $w_{26}$ | 0.020 | 0.085 | 0.153 | 0.033 | 0.057 | 0.041 | 0.021 | 0.016 | -0.058 |
| $w_{27}$ | 0.076 | 0.012 | -0.064 | 0.055 | -0.263 | -0.055 | 0.176 | -0.012 | -0.090 |
| $w_{28}$ | 0.113 | -0.009 | -0.064 | -0.094 | 0.121 | 0.130 | -0.027 | -0.032 | 0.133 |
| $w_{29}$ | 0.121 | 0.137 | 0.007 | -0.080 | 0.032 | 0.121 | 0.016 | -0.146 | 0.133 |
| $w_{30}$ | -0.504 | -0.587 | 0.209 | -0.022 | -0.187 | -0.109 | 0.008 | 0.164 | -0.927 |
| $C$ | 0.185 | -1.832 | 0.105 | 0.178 | 1.082 | 0.661 | 1.034 | 0.300 | -0.868 |

where $w_{i=1,\ldots,30}$ are the hidden layer node weights and $C$ is the bias and are determined using Table 7.4. Note that $w_{i=1,\ldots,30}$ and $C$ are dimensionless.

For $\tilde{N}_c$, the optimal MLP model is expressed as follows:

$$\tilde{N}_c = \left[ \frac{2.306}{1+\exp\begin{pmatrix} 6.979T_1 - 2.655T_2 - 2.305T_3 - 2.281T_4 \\ +1.683T_5 - 1.972T_6 + 4.518T_7 + 3.157T_8 \\ -2.110T_9 - 2.818 \end{pmatrix}} + 0.174 \right] \tag{7.14}$$

where $T_{i=1,\ldots9}$ are calculated as:

$$T_{i=1,\ldots,9} = \left[ 1+\exp\begin{pmatrix} w_1 c_1 + w_2 c_2 + w_3 c_3 + w_4 c_4 + w_5 c_5 + w_6 c_6 \\ + w_7 c_7 + w_8 c_8 + w_9 c_9 + w_{10} c_{10} + w_{11} h_1 \\ + w_{12} h_2 + w_{13} h_3 + w_{14} h_4 + w_{15} h_5 + w_{16} h_6 \\ + w_{17} h_7 + w_{18} h_8 + w_{19} h_9 + w_{20} B + C \end{pmatrix} \right]^{-1} \tag{7.15}$$

where $w_{i=1,\ldots,20}$ and $C$ are determined using Table 7.5.

For $\tilde{N}_{c-\phi}$, the optimal MLP model is expressed as follows:

$$\tilde{N}_{c-\phi} = \left[ \frac{2.511}{1+\exp\begin{pmatrix} 1.432T_1 - 1.254T_2 + 0.789T_3 - 1.952T_4 \\ +0.898T_5 - 1.009T_6 + 0.289T_7 - 1.017T_8 \\ +0.593T_9 - 0.335 \end{pmatrix}} + 0.524 \right] \tag{7.16}$$

where $T_{i=1,\ldots9}$ are calculated as:

$$T_{i=1,\ldots,9} = \tanh\begin{pmatrix} w_1 c_1 + w_2 c_2 + w_3 c_3 + w_4 c_4 + w_5 c_5 + w_6 c_6 \\ + w_7 c_7 + w_8 c_8 + w_9 c_9 + w_{10} c_{10} + w_{11} \phi_1 \\ + w_{12} \phi_2 + w_{13} \phi_3 + w_{14} \phi_4 + w_{15} \phi_5 + w_{16} \phi_6 \\ + w_{17} \phi_7 + w_{18} \phi_8 + w_{19} \phi_9 + w_{20} \phi_{10} + w_{21} h_1 \\ + w_{22} h_2 + w_{23} h_3 + w_{24} h_4 + w_{25} h_5 + w_{26} h_6 \\ + w_{27} h_7 + w_{28} h_8 + w_{29} h_9 + w_{30} B + C \end{pmatrix} \tag{7.17}$$

where $w_{i=1,\ldots,30}$ and $C$ are determined using Table 7.6.

**Table 7.5** Values of $w_{i=1,\ldots,20}$ and $C$ versus $T_{i=1,\ldots,9}$ for $\tilde{N}_c$.

| | $T_1$ | $T_2$ | $T_3$ | $T_4$ | $T_5$ | $T_6$ | $T_7$ | $T_8$ | $T_9$ |
|---|---|---|---|---|---|---|---|---|---|
| $w_1$ | -0.777 | -0.098 | -0.091 | -0.313 | -0.239 | 0.097 | -0.046 | -0.502 | -0.238 |
| $w_2$ | 0.027 | -0.002 | 0.039 | 0.042 | -0.161 | 0.228 | 0.622 | 0.210 | -0.085 |
| $w_3$ | 0.016 | 0.013 | -0.181 | 0.402 | -0.002 | -0.164 | -0.075 | 0.170 | -0.036 |
| $w_4$ | -0.018 | -0.060 | -0.075 | -0.044 | 0.055 | -0.064 | -0.014 | 0.045 | 0.281 |
| $w_5$ | 0.026 | -0.041 | 0.051 | 0.013 | 0.077 | -0.024 | -0.030 | 0.026 | 0.086 |
| $w_6$ | 0.012 | -0.034 | 0.034 | 0.021 | 0.066 | -0.022 | -0.027 | 0.016 | 0.062 |
| $w_7$ | 0.024 | -0.015 | 0.010 | 0.004 | 0.022 | -0.011 | -0.015 | 0.011 | 0.037 |
| $w_8$ | 0.005 | -0.002 | 0.003 | 0.003 | 0.017 | -0.007 | -0.002 | 0.000 | 0.009 |
| $w_9$ | 0.006 | -0.009 | -0.007 | 0.008 | 0.008 | -0.012 | -0.010 | -0.006 | 0.012 |
| $w_{10}$ | -0.004 | 0.005 | 0.022 | -0.006 | 0.013 | -0.023 | -0.019 | -0.004 | 0.007 |
| $w_{11}$ | -7.062 | -0.775 | -1.067 | 1.508 | -1.834 | -0.298 | 1.876 | 1.069 | 1.185 |
| $w_{12}$ | 0.038 | -0.351 | -0.918 | 0.503 | -0.234 | 0.102 | -1.095 | 0.542 | 0.533 |
| $w_{13}$ | -0.238 | 0.664 | 0.299 | -0.840 | -0.432 | -1.421 | 0.031 | 0.045 | 1.059 |
| $w_{14}$ | -0.015 | 0.063 | 0.325 | 0.262 | 0.064 | -0.153 | -0.112 | 0.045 | -0.331 |
| $w_{15}$ | 0.076 | -0.115 | -0.007 | -0.047 | 0.238 | 0.157 | -0.094 | 0.013 | 0.184 |
| $w_{16}$ | -0.080 | 0.097 | -0.100 | -0.011 | -0.035 | 0.010 | -0.072 | 0.029 | -0.079 |
| $w_{17}$ | -0.169 | 0.044 | -0.108 | -0.031 | -0.042 | 0.143 | 0.070 | 0.006 | -0.106 |
| $w_{18}$ | -0.352 | 0.153 | -0.131 | -0.105 | -0.063 | -0.033 | 0.121 | -0.002 | -0.022 |
| $w_{19}$ | -0.045 | 0.136 | 0.034 | 0.038 | -0.115 | -0.383 | -0.087 | -0.027 | 0.019 |
| $w_{20}$ | 0.473 | 0.356 | -0.048 | -0.536 | 0.750 | 0.305 | -0.152 | -0.574 | -0.561 |
| $C$ | 0.350 | 1.489 | 0.274 | -1.099 | -0.842 | 0.734 | 1.606 | 0.377 | -1.782 |

**Table 7.6** Values of $w_{i=1,\ldots,30}$ and $C$ versus $T_{i=1,\ldots,9}$ for $\tilde{N}_{c-\phi}$.

| | $T_1$ | $T_2$ | $T_3$ | $T_4$ | $T_5$ | $T_6$ | $T_7$ | $T_8$ | $T_9$ |
|---|---|---|---|---|---|---|---|---|---|
| $w_1$ | -0.163 | -0.107 | 0.045 | -0.362 | -0.007 | -0.029 | 0.038 | -0.035 | 0.000 |
| $w_2$ | 0.090 | -0.008 | -0.054 | 0.028 | -0.172 | 0.011 | 0.018 | -0.072 | 0.003 |
| $w_3$ | 0.042 | 0.018 | -0.054 | 0.050 | 0.092 | -0.053 | 0.060 | 0.077 | -0.125 |
| $w_4$ | 0.025 | 0.029 | -0.013 | 0.033 | 0.054 | 0.014 | -0.076 | 0.067 | 0.107 |
| $w_5$ | -0.026 | 0.019 | 0.038 | 0.023 | 0.011 | -0.016 | 0.019 | 0.003 | -0.004 |
| $w_6$ | -0.005 | 0.021 | 0.025 | 0.005 | 0.020 | 0.020 | -0.001 | 0.006 | 0.028 |
| $w_7$ | 0.002 | 0.009 | 0.009 | -0.014 | 0.001 | -0.016 | -0.005 | 0.025 | 0.007 |
| $w_8$ | 0.000 | 0.011 | 0.012 | 0.001 | 0.009 | 0.013 | 0.030 | 0.008 | 0.011 |
| $w_9$ | 0.015 | 0.017 | 0.008 | -0.011 | 0.019 | 0.017 | 0.024 | 0.013 | -0.005 |
| $w_{10}$ | 0.009 | 0.002 | -0.008 | -0.010 | -0.007 | 0.000 | -0.003 | -0.007 | -0.020 |
| $w_{11}$ | 0.049 | -0.100 | 0.009 | 0.052 | -0.019 | 0.050 | 0.023 | 0.037 | -0.002 |
| $w_{12}$ | -0.008 | 0.027 | -0.067 | 0.011 | 0.067 | 0.048 | -0.026 | -0.035 | 0.018 |
| $w_{13}$ | -0.015 | 0.008 | -0.044 | 0.009 | -0.008 | -0.061 | -0.015 | 0.035 | 0.041 |
| $w_{14}$ | -0.011 | 0.018 | 0.020 | -0.003 | -0.001 | -0.006 | 0.030 | -0.006 | -0.026 |
| $w_{15}$ | 0.013 | 0.019 | 0.012 | -0.020 | -0.004 | 0.014 | -0.022 | -0.003 | 0.004 |
| $w_{16}$ | -0.007 | 0.008 | 0.023 | 0.009 | -0.008 | -0.003 | -0.016 | -0.009 | -0.001 |
| $w_{17}$ | -0.002 | 0.008 | 0.001 | 0.000 | 0.003 | -0.011 | -0.025 | 0.002 | 0.011 |
| $w_{18}$ | -0.004 | 0.005 | 0.015 | 0.006 | -0.011 | -0.003 | -0.012 | -0.015 | -0.007 |
| $w_{19}$ | 0.003 | 0.011 | 0.004 | -0.006 | 0.011 | 0.007 | 0.041 | 0.016 | 0.008 |
| $w_{20}$ | 0.000 | 0.000 | 0.016 | -0.004 | -0.007 | -0.003 | 0.000 | -0.001 | -0.022 |
| $w_{21}$ | 0.249 | 0.598 | -0.025 | -0.255 | -0.746 | -0.666 | 0.599 | -0.756 | -0.729 |
| $w_{22}$ | 0.262 | 0.112 | 0.677 | -0.364 | 0.367 | -0.232 | -0.325 | 0.775 | -0.546 |
| $w_{23}$ | 0.194 | 0.135 | 0.429 | -0.131 | 0.282 | 0.444 | -0.613 | 0.062 | 0.035 |
| $w_{24}$ | 0.181 | 0.188 | -0.130 | -0.016 | 0.210 | 0.205 | -0.050 | 0.068 | 0.258 |
| $w_{25}$ | -0.072 | -0.065 | -0.070 | -0.014 | -0.090 | -0.145 | 0.276 | 0.024 | -0.096 |
| $w_{26}$ | 0.050 | -0.057 | 0.016 | -0.043 | -0.260 | -0.024 | 0.080 | -0.119 | -0.128 |
| $w_{27}$ | 0.021 | 0.039 | -0.035 | 0.072 | 0.171 | 0.139 | -0.076 | 0.094 | 0.261 |
| $w_{28}$ | -0.130 | -0.109 | -0.041 | 0.235 | -0.134 | 0.192 | 0.521 | -0.163 | 0.135 |
| $w_{29}$ | 0.102 | 0.000 | 0.051 | -0.124 | -0.208 | 0.108 | -0.382 | -0.002 | 0.329 |
| $w_{30}$ | -0.114 | -0.241 | -0.210 | 0.155 | 0.022 | 0.139 | 0.049 | 0.014 | 0.109 |
| $C$ | -0.019 | 0.404 | -0.538 | -1.640 | 0.185 | -0.111 | -0.299 | -0.428 | 0.058 |

## 7.6 SENSITIVITY AND ROBUSTNESS OF THE MLP-BASED BEARING CAPACITY EQUATIONS

The robustness of the design equations, which were presented in the previous section, is determined by examining how well the predicted bearing capacity agrees with the underlying physical behaviour of the bearing capacity of a shallow strip footing. In order to test the robustness of MLP-based bearing capacity formulae, sensitivity analyses were carried out. The sensitivity analyses were used to investigate the response of the predicted bearing capacity from the design equations to a set of hypothetical input data.

Because ANN-based models work best when used in interpolation, the input data was generated over the range of the minimum and maximum of the data used for MLP model training. All input variables, except the one chosen to be varied, were fixed to a given value. Hence, a set of synthetic data was generated by increasing the given variable within this range. The generated inputs were then presented to the design equations and the bearing capacity calculated. This process was repeated by choosing another variable as the single varied input until the model response was tested for all input variables.

The inputs employed in the sensitivity analyses, and the corresponding responses from the MLP models, are presented in the following subsections, which are categorized depending on the input variables. The sensitivity analyses of $c_i$ are presented in section 7.6.1, while the results for $\phi_i$, $h_i$ and $B$ are presented in sections 7.6.2 to 7.6.4, respectively.

### 7.6.1 Variation of Predicted $q_{u(c\text{-}\phi)}$ with Respect to Variation of $c$ in each of the 10 Layers

In this section, the results of sensitivity analyses carried out on the soil cohesion, $c_i$ are presented. The inputs for $c_i$ for each of ten cases are presented in Table 7.7. In Case 1, for example, the soil cohesion of the uppermost layer, $c_1$, is varied from 1.0 to 10.0, while the cohesion of the remaining 9 layers are fixed at a value of 10.0. The values for $\phi_i$, $h_i$ and $B$ are fixed at values of 20.0°, 0.5 m and 2.5 m, respectively, in all

ten cases. These inputs are then input in equations, and $q_{u(c\text{-}\phi)}$ calculated: one determined by Equations 7.12 and 7.13; and another using Equations 7.14 to 7.17. The results for Case 1 are then plotted as continuous lines as shown in Figures 7.10 and 7.11. This process is repeated for all cases.

**Table 7.7** A set of hypothetical data employed to analyse the sensitivity of $c_i$.

| Case | $c_1$ (kPa) | $c_2$ (kPa) | $c_3$ (kPa) | $c_4$ (kPa) | $c_5$ (kPa) | $c_6$ (kPa) | $c_7$ (kPa) | $c_8$ (kPa) | $c_9$ (kPa) | $c_{10}$ (kPa) |
|---|---|---|---|---|---|---|---|---|---|---|
| **1** | $1.0<c_1<10.0$ | 10.0 | 10.0 | 10.0 | 10.0 | 10.0 | 10.0 | 10.0 | 10.0 | 10.0 |
| **2** | 10.0 | $1.0<c_2<10.0$ | 10.0 | 10.0 | 10.0 | 10.0 | 10.0 | 10.0 | 10.0 | 10.0 |
| **3** | 10.0 | 10.0 | $1.0<c_3<10.0$ | 10.0 | 10.0 | 10.0 | 10.0 | 10.0 | 10.0 | 10.0 |
| **4** | 10.0 | 10.0 | 10.0 | $1.0<c_4<10.0$ | 10.0 | 10.0 | 10.0 | 10.0 | 10.0 | 10.0 |
| **5** | 10.0 | 10.0 | 10.0 | 10.0 | $1.0<c_5<10.0$ | 10.0 | 10.0 | 10.0 | 10.0 | 10.0 |
| **6** | 10.0 | 10.0 | 10.0 | 10.0 | 10.0 | $1.0<c_6<10.0$ | 10.0 | 10.0 | 10.0 | 10.0 |
| **7** | 10.0 | 10.0 | 10.0 | 10.0 | 10.0 | 10.0 | $1.0<c_7<10.0$ | 10.0 | 10.0 | 10.0 |
| **8** | 10.0 | 10.0 | 10.0 | 10.0 | 10.0 | 10.0 | 10.0 | $1.0<c_8<10.0$ | 10.0 | 10.0 |
| **9** | 10.0 | 10.0 | 10.0 | 10.0 | 10.0 | 10.0 | 10.0 | 10.0 | $1.0<c_9<10.0$ | 10.0 |
| **10** | 10.0 | 10.0 | 10.0 | 10.0 | 10.0 | 10.0 | 10.0 | 10.0 | 10.0 | $1.0<c_{10}<10.0$ |

The results, shown in Figures 7.10 and 7.11, indicate that, for Case 1, as the soil strength of the uppermost layer increases, $q_{u(c\text{-}\phi)}$ also increases. This observation is in good agreement with what one would expect based on the physical problem. In general, Cases 2 to 7 demonstrate the same model responses as for Case 1, while Cases 8 to 10 illustrate that $q_{u(c\text{-}\phi)}$ is stable, or changes little as the soil cohesion in layers 8 to 10 increases. This is appropriate if the variation of $c_i$ occurs at a depth that is beyond the depth of the influence zone of the footing.

Interestingly, it can be seen that the estimates of $q_{u(c\text{-}\phi)}$ plateaus at different levels, as illustrated in Figures 7.10 and 7.11, which are lower than the theoretical estimates. Theoretically, $q_{u(c\text{-}\phi)}$ should reach approximately 148.5 kN/m$^2$ by using Equations 7.2 and 7.3, and 142.5 kN/m$^2$ if finite element lower bound analysis is used, for $c_i$ = 10.0 kPa and $\phi_i$ = 20.0°. The explanation of this numerical inaccuracy lies within the training data presented for ANN training. The case, where all the soil layers have the same $c_i$ = 10.0 kPa and $\phi_i$ = 20.0°, never occurs in the Monte Carlo analysis. Consequently, the *known* maximum value of $q_{u(c\text{-}\phi)}$, which is only 93.31 kN/m$^2$ (shown in Table C.1 in Appendix C), is the upper limit of the estimates that can be obtained from Equations 7.12 and 7.13. The maximum values of known $\tilde{N}_c$ and $\tilde{N}_{c-\phi}$ also affect the upper limit of $q_{u(c\text{-}\phi)}$ obtained from Equations 7.14 to 7.17. Thus, these numerical errors highlight the vulnerability and limitation of the MLP-based equations. Whilst, this error is undesirable, the ANN-based model is developed primarily to predict the bearing capacity of soil layers having different values $c_i$ and $\phi_i$.

### 7.6.2 Variation of Predicted $q_{u(c\text{-}\phi)}$ with Respect to Variation of $\phi$ in Each of the 10 Layers

In this Section, sensitivity analyses are carried out on $\phi_i$ using the methodology described earlier. The hypothetical inputs employed in the sensitivity analyses for 10

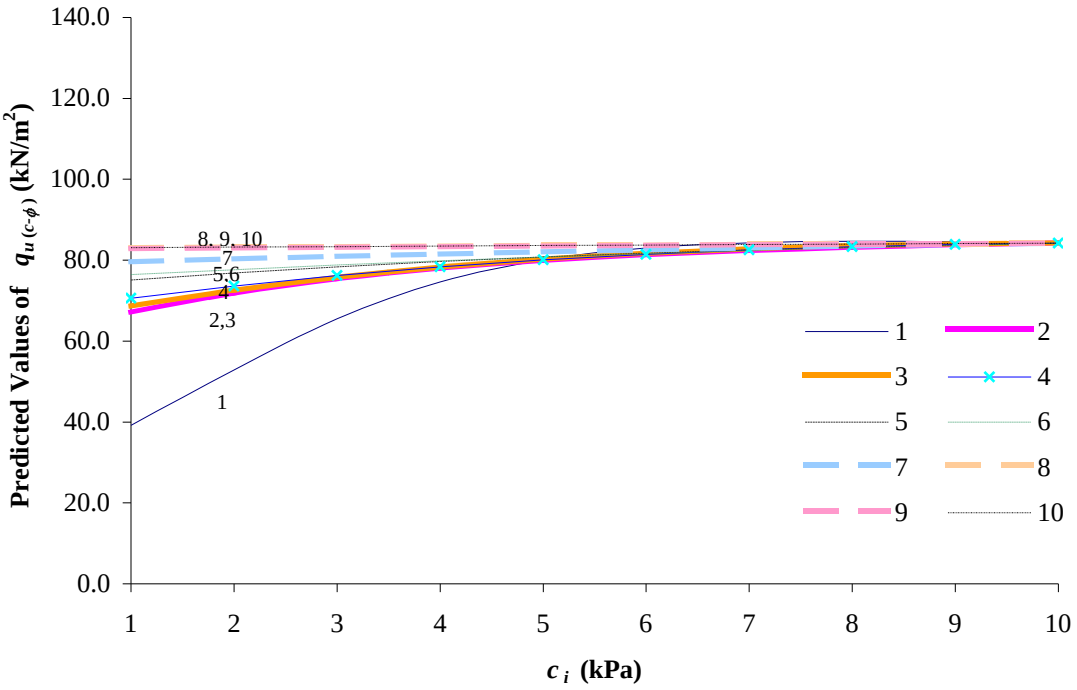


**Figure 7.10** Variation of $q_{u(c\text{-}\phi)}$ due to varying soil cohesion, $c_i$. ($q_{u(c\text{-}\phi)}$ is determined by Equations 7.12 and 7.13)

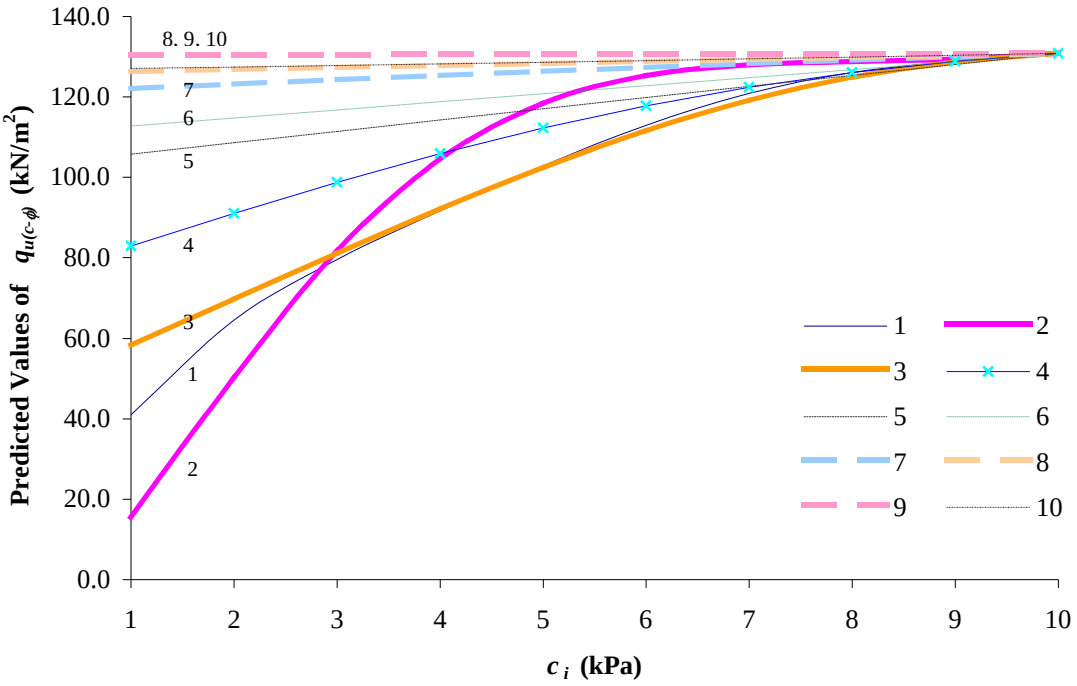


**Figure 7.11** Variation of $q_{u(c\text{-}\phi)}$ with varying soil cohesion, $c_i$. ($q_{u(c\text{-}\phi)}$ is determined by Equations 7.14 to 7.17)

**Table 7.8** A set of hypothetical data employed to analyse the sensitivity of $\phi_i$.

| Case | $\phi_1$ (°) | $\phi_2$ (°) | $\phi_3$ (°) | $\phi_4$ (°) | $\phi_5$ (°) | $\phi_6$ (°) | $\phi_7$ (°) | $\phi_8$ (°) | $\phi_9$ (°) | $\phi_{10}$ (°) |
|---|---|---|---|---|---|---|---|---|---|---|
| **1** | 5.0<$\phi_1$<20.0 | 20.0 | 20.0 | 20.0 | 20.0 | 20.0 | 20.0 | 20.0 | 20.0 | 20.0 |
| **2** | 20.0 | 5.0<$\phi_2$<20.0 | 20.0 | 20.0 | 20.0 | 20.0 | 20.0 | 20.0 | 20.0 | 20.0 |
| **3** | 20.0 | 20.0 | 5.0<$\phi_3$<20.0 | 20.0 | 20.0 | 20.0 | 20.0 | 20.0 | 20.0 | 20.0 |
| **4** | 20.0 | 20.0 | 20.0 | 5.0<$\phi_4$<20.0 | 20.0 | 20.0 | 20.0 | 20.0 | 20.0 | 20.0 |
| **5** | 20.0 | 20.0 | 20.0 | 20.0 | 5.0<$\phi_5$<20.0 | 20.0 | 20.0 | 20.0 | 20.0 | 20.0 |
| **6** | 20.0 | 20.0 | 20.0 | 20.0 | 20.0 | 5.0<$\phi_1$<20.0 | 20.0 | 20.0 | 20.0 | 20.0 |
| **7** | 20.0 | 20.0 | 20.0 | 20.0 | 20.0 | 20.0 | 5.0<$\phi_1$<20.0 | 20.0 | 20.0 | 20.0 |
| **8** | 20.0 | 20.0 | 20.0 | 20.0 | 20.0 | 20.0 | 20.0 | 5.0<$\phi_1$<20.0 | 20.0 | 20.0 |
| **9** | 20.0 | 20.0 | 20.0 | 20.0 | 20.0 | 20.0 | 20.0 | 20.0 | 5.0<$\phi_1$<20.0 | 20.0 |
| **10** | 20.0 | 20.0 | 20.0 | 20.0 | 20.0 | 20.0 | 20.0 | 20.0 | 20.0 | 5.0<$\phi_{10}$<20.0 |

cases are presented in Table 7.8. The values for $c_i$, $h_i$ and $B$ are fixed at values of 5.0 kN/m$^2$, 1.0 m and 2.5 m, respectively. The results of the sensitivity analyses are presented in Figures 7.12 and 7.13.

It can been seen from Figures 7.12 and 7.13, that $q_{u(c\text{-}\phi)}$ increases as the soil shear strength increases. For example, the friction angle of the uppermost layer, $\phi_1$, is

varied from 5.0° to 20.0° in Case 1, while the $\phi_i$ of other nine layers are fixed at a value of 20.0°. When Equations 7.12 and 7.13 are employed, $q_{u(c\text{-}\phi)}$ increases from 47.5 kN/m$^2$ to 63.2 kN/m$^2$ as $\phi_1$ increases from 5.0° to 20.0°, and $q_{u(c\text{-}\phi)}$ increases from 31.4 kN/m$^2$ to 67.6 kN/m$^2$ when Equations 7.14 to 7.17 are used. Despite the difference in the estimation of $q_{u(c\text{-}\phi)}$ resulting from the different MLP models employed, in general, the variations shown in Figures 7.12 and 7.13 agree with the expected variation of the bearing capacity. In some cases (for example, Cases 8 to 10, in Figure 7.12, and Cases 6 to 10, in Figure 7.12), it can be seen that the variation of $\phi_i$ has very little effect on $q_{u(c\text{-}\phi)}$ since the variation takes place at a depth which is beyond the depth of the influence zone. As a result of the numerical errors, which were discussed in the previous section, $q_{u(c\text{-}\phi)}$ plateaus at a level below 70.0 kN/m$^2$, and less than the theoretical estimate of approximately 74.3 kN/m$^2$ by using Equations 7.2 and 7.3, and 74.0 kN/m$^2$ if finite element lower bound analysis is used, when $c_i$ and $\phi_i$ of all 10 layers have the same values of 5.0 kN/m$^2$ and 20.0°, respectively.

### 7.6.3 Variation of Predicted Value of $q_{u(c\text{-}\phi)}$ with Respect to Variation of $h_i$ in Each of the 10 Layers

Variation of $h_i$ alone requires careful attention. If $c_i$ and $\phi_i$ are assigned the same values, the variation of $h_i$ alone will not affect $q_{u(c\text{-}\phi)}$. Hence, it is proposed that the values of $c_i$ and $\phi_i$ of the layer where the variation of $h_i$ occurs, are assigned different values. The hypothetical inputs for $c_i$, $\phi_i$ and $h_i$ employed in the sensitivity analyses for 10 cases are presented in Table 7.9. The footing width, $B$ = 2.5 m is used in the analyses. The results of the sensitivity analyses are presented in Figures 7.14 and 7.15.

The results shown in Figures 7.14 and 7.15 indicate that there are differences in $q_{u(c\text{-}\phi)}$ obtained from the two MLP models. This could be the result of different initial random weights used during training. In addition, due to the two different ways of expressing $q_{u(c\text{-}\phi)}$, there are differences in the network architecture and therefore the ANN yields vastly different networks, and hence, the predictions of $q_{u(c\text{-}\phi)}$.

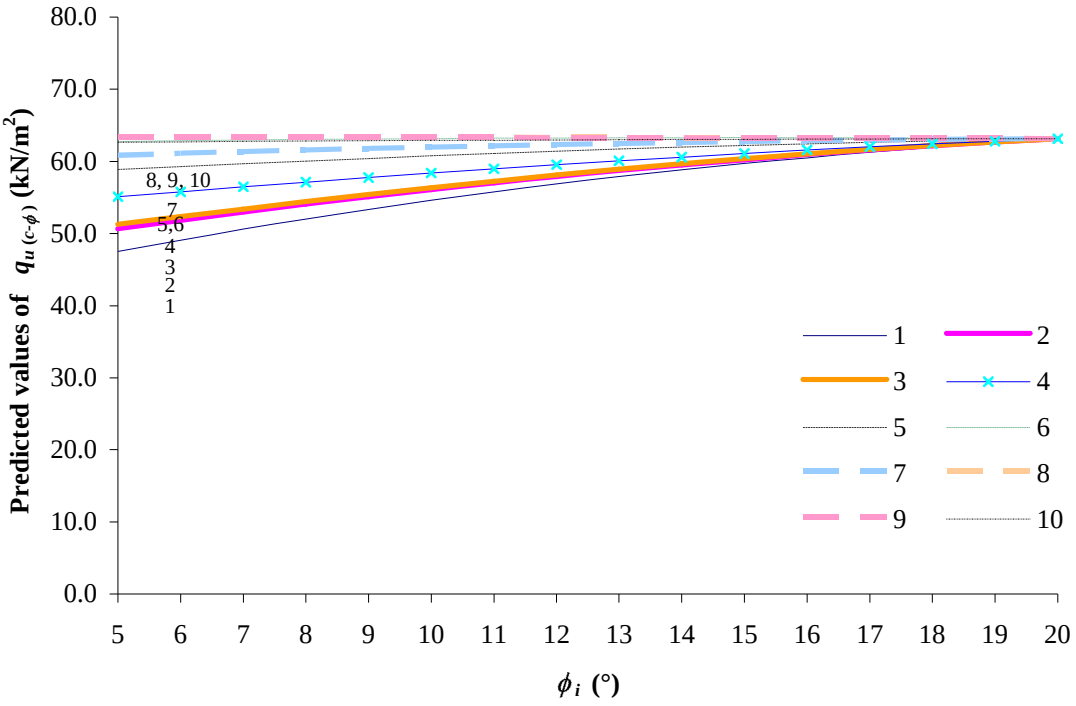


**Figure 7.12** Variation of $q_{u(c-\phi)}$ due to varying friction angle, $\phi_i$. ($q_{u(c-\phi)}$ is determined by Equations 7.12 and 7.13)

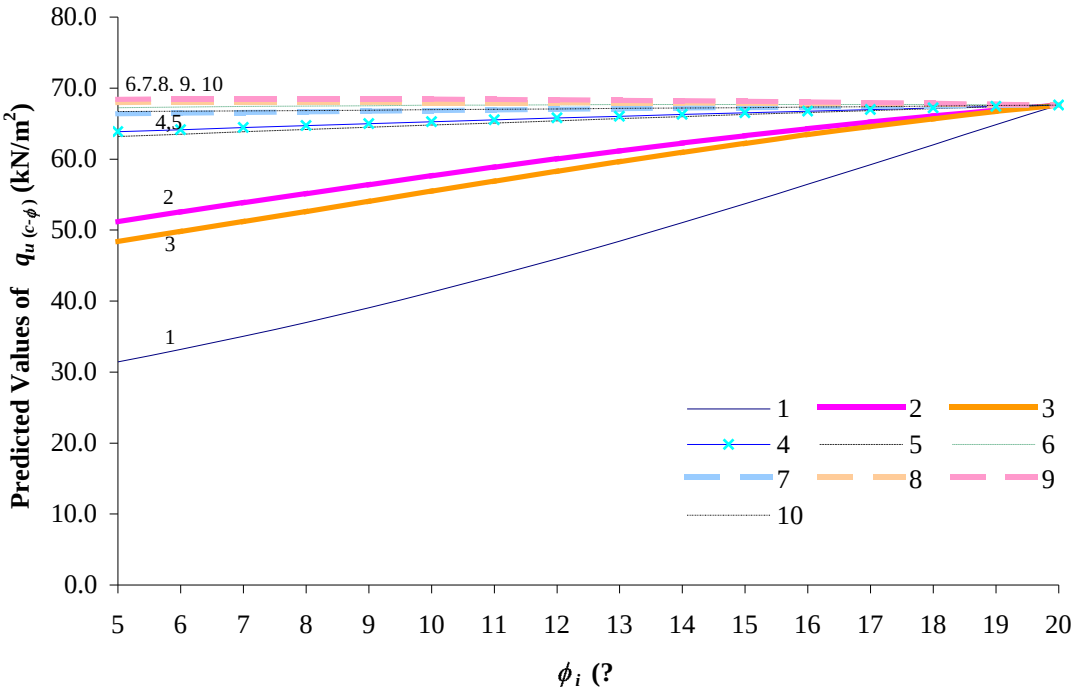


**Figure 7.13** Variation of $q_{u(c-\phi)}$ with varying friction angle, $\phi_i$. ($q_{u(c-\phi)}$ is determined by Equations 7.14 to 7.17)

**Table 7.9** A set of hypothetical data employed to analyse the sensitivity of $h_i$.

| Case | $h_1$ (m) | $h_2$ (m) | $h_3$ (m) | $h_4$ (m) | $h_5$ (m) | $h_6$ (m) | $h_7$ (m) | $h_8$ (m) | $h_9$ (m) |
|---|---|---|---|---|---|---|---|---|---|
| **1** | $0.2<h_1<1.0$ | 0.2 | 0.2 | 0.2 | 0.2 | 0.2 | 0.2 | 0.2 | 0.2 |
| **2** | 0.2 | $0.2<h_2<1.0$ | 0.2 | 0.2 | 0.2 | 0.2 | 0.2 | 0.2 | 0.2 |
| **3** | 0.2 | 0.2 | $0.2<h_3<1.0$ | 0.2 | 0.2 | 0.2 | 0.2 | 0.2 | 0.2 |
| **4** | 0.2 | 0.2 | 0.2 | $0.2<h_4<1.0$ | 0.2 | 0.2 | 0.2 | 0.2 | 0.2 |
| **5** | 0.2 | 0.2 | 0.2 | 0.2 | $0.2<h_5<1.0$ | 0.2 | 0.2 | 0.2 | 0.2 |
| **6** | 0.2 | 0.2 | 0.2 | 0.2 | 0.2 | $0.2<h_6<1.0$ | 0.2 | 0.2 | 0.2 |
| **7** | 0.2 | 0.2 | 0.2 | 0.2 | 0.2 | 0.2 | $0.2<h_7<1.0$ | 0.2 | 0.2 |
| **8** | 0.2 | 0.2 | 0.2 | 0.2 | 0.2 | 0.2 | 0.2 | $0.2<h_8<1.0$ | 0.2 |
| **9** | 0.2 | 0.2 | 0.2 | 0.2 | 0.2 | 0.2 | 0.2 | 0.2 | $0.2<h_9<1.0$ |

Despite the differences in the output of the MLP models as shown in Figures 7.14 and 7.15, the trend lines are in good agreement with one would expect when analysing the bearing capacity problem of a shallow strip footing. In Case 1, for example, the shear strength of the uppermost layer is assigned to be the weakest of all layers. The thickness of layer 1, $h_1$, is varied from a minimum value of 0.2 m to a maximum value of 1.0 m (refer to Table 7.9). As $h_1$ increases, $q_{u(c\text{-}\phi)}$ decreases as shown in Figures

**Table 7.9** A set of hypothetical data employed to analyse the sensitivity of $h_i$. ***(Continued)***

| Case | $c_1$ (kPa) $\phi_1$ (°) | $c_2$ (kPa) $\phi_2$ (°) | $c_3$ (kPa) $\phi_3$ (°) | $c_4$ (kPa) $\phi_4$ (°) | $c_5$ (kPa) $\phi_5$ (°) | $c_6$ (kPa) $\phi_6$ (°) | $c_7$ (kPa) $\phi_7$ (°) | $c_8$ (kPa) $\phi_8$ (°) | $c_9$ (kPa) $\phi_9$ (°) |
|---|---|---|---|---|---|---|---|---|---|
| **1** | {1.0,5.0} | {5.0,10.0} | {5.0,10.0} | {5.0,10.0} | {5.0,10.0} | {5.0,10.0} | {5.0,10.0} | {5.0,10.0} | {5.0,10.0} |
| **2** | {5.0,10.0} | {1.0,5.0} | {5.0,10.0} | {5.0,10.0} | {5.0,10.0} | {5.0,10.0} | {5.0,10.0} | {5.0,10.0} | {5.0,10.0} |
| **3** | {5.0,10.0} | {5.0,10.0} | {1.0,5.0} | {5.0,10.0} | {5.0,10.0} | {5.0,10.0} | {5.0,10.0} | {5.0,10.0} | {5.0,10.0} |
| **4** | {5.0,10.0} | {5.0,10.0} | {5.0,10.0} | {1.0,5.0} | {5.0,10.0} | {5.0,10.0} | {5.0,10.0} | {5.0,10.0} | {5.0,10.0} |
| **5** | {5.0,10.0} | {5.0,10.0} | {5.0,10.0} | {5.0,10.0} | {1.0,5.0} | {5.0,10.0} | {5.0,10.0} | {5.0,10.0} | {5.0,10.0} |
| **6** | {5.0,10.0} | {5.0,10.0} | {5.0,10.0} | {5.0,10.0} | {5.0,10.0} | {1.0,5.0} | {5.0,10.0} | {5.0,10.0} | {5.0,10.0} |
| **7** | {5.0,10.0} | {5.0,10.0} | {5.0,10.0} | {5.0,10.0} | {5.0,10.0} | {5.0,10.0} | {1.0,5.0} | {5.0,10.0} | {5.0,10.0} |
| **8** | {5.0,10.0} | {5.0,10.0} | {5.0,10.0} | {5.0,10.0} | {5.0,10.0} | {5.0,10.0} | {5.0,10.0} | {1.0,5.0} | {5.0,10.0} |
| **9** | {5.0,10.0} | {5.0,10.0} | {5.0,10.0} | {5.0,10.0} | {5.0,10.0} | {5.0,10.0} | {5.0,10.0} | {5.0,10.0} | {1.0,5.0} |

7.14 and 7.15. It can be seen from these figures that this observation is also valid for some cases (i.e. Cases 2 to 5), whilst in other cases, such as Cases 6 to 8, the decreasing trend is less obvious.

### 7.6.4 Variation of Predicted $q_{u(c\text{-}\phi)}$ with Respect to Variation of $B$

Three cases are considered to test the model responses with respect to the input variable $B$, namely decreasing shear strength with depth, constant shear strength, and

increasing shear strength with depth. An illustration of the three cases that are considered in the sensitivity analyses and the synthetic inputs are shown in Figure 7.16. The results of the analyses are shown in Figures 7.17 and 7.18.

Theoretically, as the footing width, $B$, increases, the depth of the influence zone also increases. Therefore, the shear strength at greater depth have an increasing effect on the bearing capacity of footing. For footings founded on soil with decreasing shear strength with depth, for example, as the footing width increases, the bearing capacity of footing reduces, as shown in Figures 7.17 and 7.18. The results also show that, if the footing is founded on soil whose shear strength increases with depth, the bearing capacity, $q_{u(c\text{-}\phi)}$, of the footing increases as the footing width increases. If the shear strength is constant with depth, the bearing capacity, $q_{u(c\text{-}\phi)}$, of the footing, however, remains constant, or varies marginally as the footing width is increased.

Overall, the results of the sensitivity analyses presented in this section, indicate that the behaviour of the MLP model agrees well with what one would expect based on the

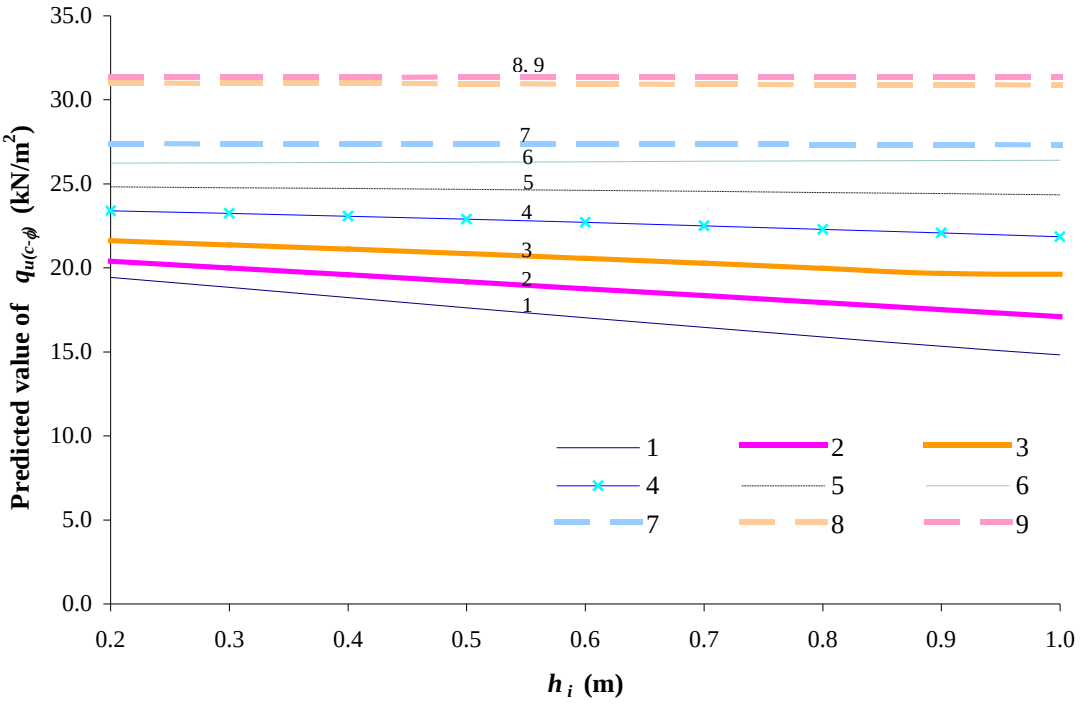


**Figure 7.14** Variation of $q_{u(c\text{-}\phi)}$ versus varying layer thickness, $h_i$. ($q_{u(c\text{-}\phi)}$ is determined by Equations 7.12 and 7.13)

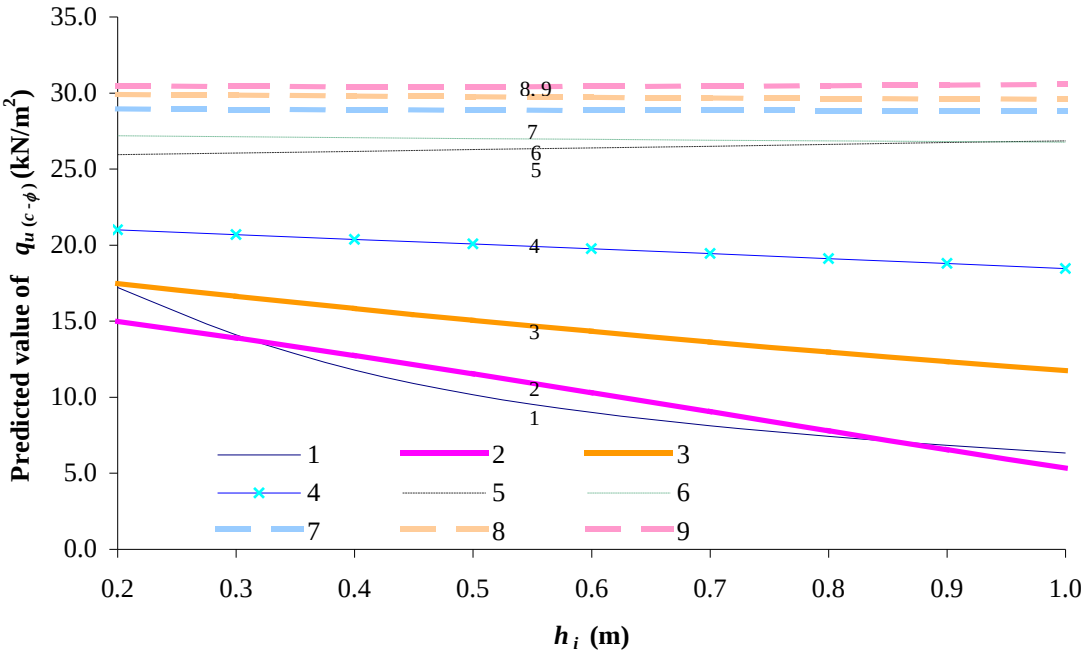


**Figure 7.15** Variation of $q_{u(c\text{-}\phi)}$ versus varying layer thickness, $h_i$. ($q_{u(c\text{-}\phi)}$ is determined by Equations 7.14 to 7.17)

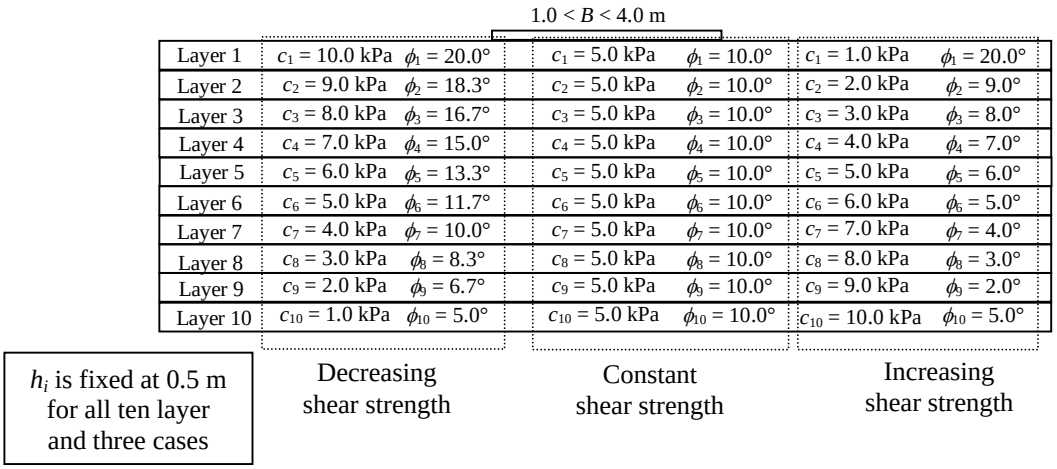


**Figure 7.16** Three cases considered in the sensitivity analyses.

underlying physical understanding of bearing capacity problem and exhibits a smooth and continuous relationship. Consequently, it is suggested that the MPL-based formulae are robust and can be used confidently for predictive purposes.

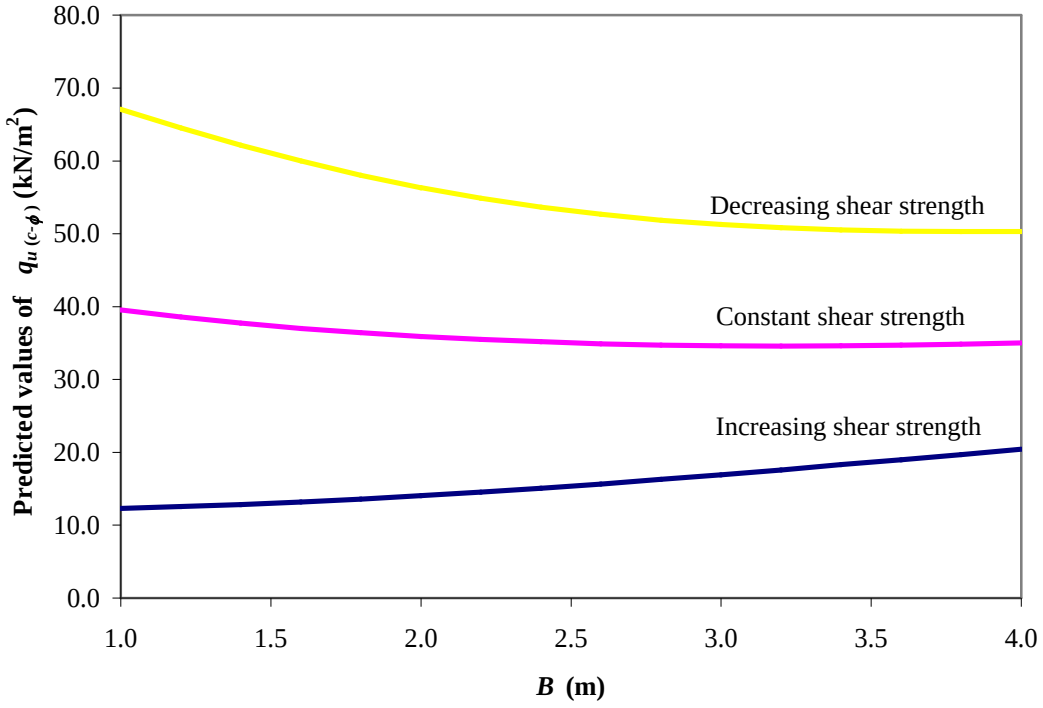


**Figure 7.17** Variation of $q_{u(c\text{-}\phi)}$ versus varying footing width, $B$. ($q_{u(c\text{-}\phi)}$ is determined by Equations 7.12 and 7.13)

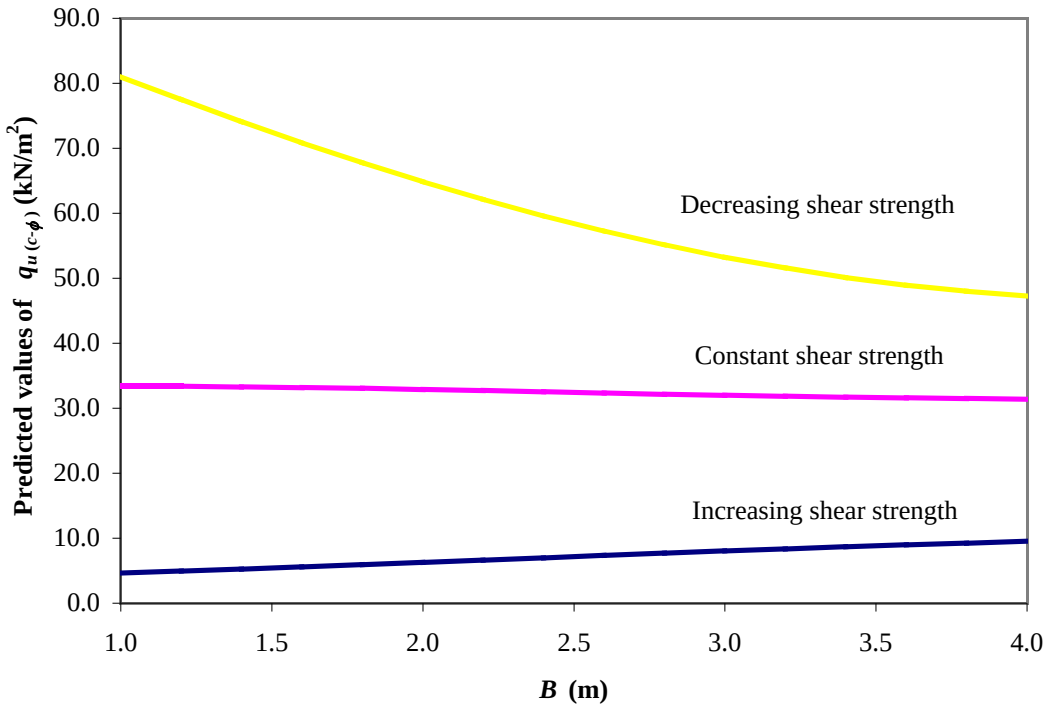


**Figure 7.18** Variation of $q_{u(c\text{-}\phi)}$ versus varying footing width, $B$. ($q_{u(c\text{-}\phi)}$ is determined by Equations 7.14 to 7.17)

# 7.7 COMPARISON OF MLP MODELS WITH CURRENT METHODS

In order to examine the accuracy and the merit of the developed MLP models, they are compared with the other available traditional methods. Unfortunately, the weighted average method (e.g. Bowles, 1988) is the only one available and the methods proposed by Davis and Booker (1973) can be only applied to relatively limited cases. The comparisons are carried out using two different cases, namely purely-cohesive and cohesive-frictional.

### 7.7.1 Foundation on 10-Layered Purely-cohesive Soil Profiles

The MLP models developed for the 10-layered purely-cohesive soil in the previous chapter are used as a comparison with the MLP models incorporating $\tilde{N}_c$ along with the weighted average method (Equations 7.4 and 7.5). The performance of the MLP models and the Bowles (1988) method are summarised in Table 7.10 and illustrated graphically in Figures 7.19 and 7.20. The results show that the MLP model with $\tilde{N}_c$ performs remarkably well, with equally high *r* values compared with the MLP model developed in the previous chapter, but with slightly lower RMSE and MAE values. Note that, the MLP model for $q_{u(c)}$ is developed using different input ranges and the average of the upper and lower bounds is used as the model target. In contrast, the MLP model with $\tilde{N}_c$, used the lower bound estimate as the model targets. As in the previous chapter, the weighted average method (Equations 7.4 and 7.5) again performed poorly and, in general, overestimated the bearing capacity, which is significant in that it provides unsafe foundation designs.

### 7.7.2 Foundation on a 10-layered Cohesive-frictional Soil Profiles

In this subsection, the predicted values of bearing capacity are calculated using the MLP model with $q_{u(c\text{-}\phi)}$, and also the MLP models with $\tilde{N}_c$ and $\tilde{N}_{c-\phi}$. Again Bowles' (1988) method is used for comparison. The performance of the MLP models and the

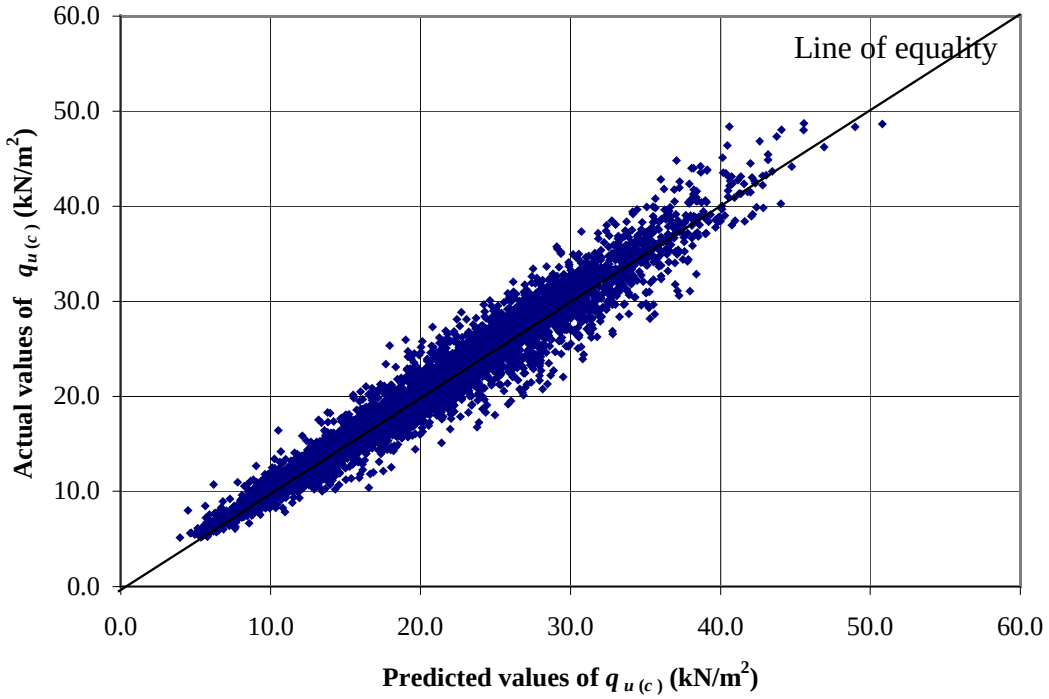


**Figure 7.19** Comparison of the bearing capacities calculated using the MLP model with $\tilde{N}_c$ versus actual values for 10-layered purely-cohesive soil.

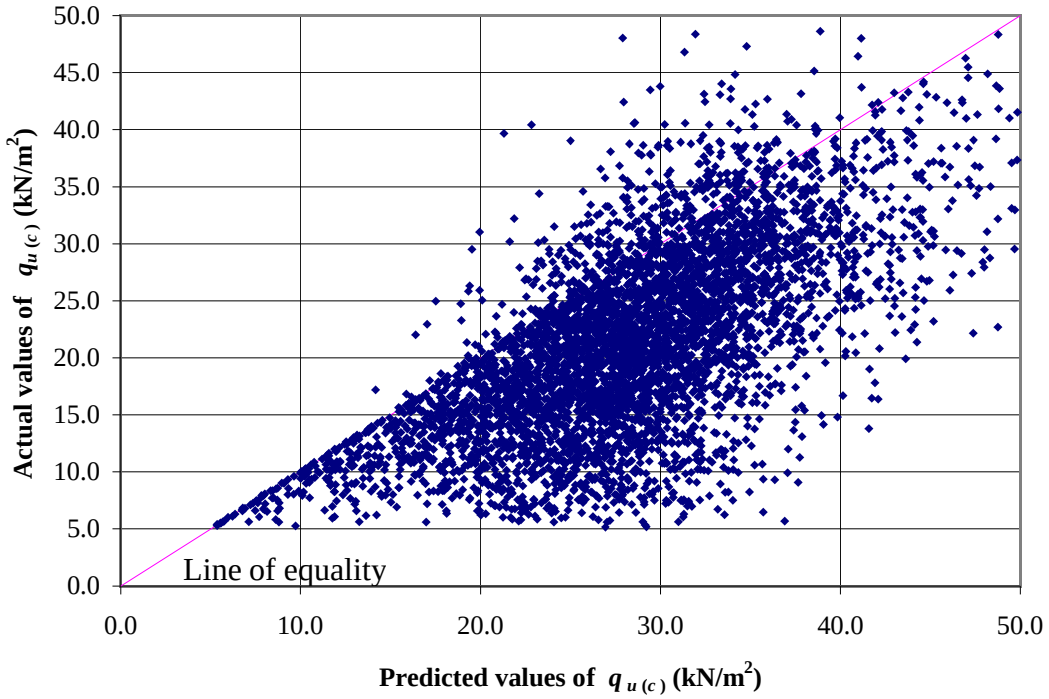


**Figure 7.20** Comparison of the bearing capacities calculated using the weighted averaging method versus actual values for purely-cohesive soil.

**Table 7.10** Comparison of MLP models and weighted-average method (Bowles, 1988) for bearing capacity prediction for purely-cohesive soil.

| Performance measurement | Methods | | |
|---|---|---|---|
| | **MLP - $q_{u(c)}$** | **MLP- $\tilde{N}_c$** | **Weighted-average method (Bowles, 1988)** |
| Correlation coefficient, *r* | 0.971 | 0.972 | 0.838 |
| RMSE (kN/m$^2$) | 2.41 | 1.89 | 8.71 |
| MAE (kN/m$^2$) | 1.64 | 1.41 | 6.94 |

Bowles (1988) method are summarised in Table 7.11 and also illustrated graphically in Figures 7.21 to 7.25. The results show that the MLP model with $q_{u(c\text{-}\phi)}$ outperforms those using $\tilde{N}_c$ and $\tilde{N}_{c-\phi}$ when predicting the bearing capacity of strip footings on cohesive-frictional soil. Table 7.11 shows that the MLP model with $q_{u(c\text{-}\phi)}$ has a slightly higher *r* value compared with the MLP models using $\tilde{N}_c$ and $\tilde{N}_{c-\phi}$, and also has lower RMSE and MAE values. In general, the predictive ability of all MLP models is satisfactory and acceptable and therefore, the use of MLP models to obtain a first estimation of the bearing capacity of a 10-layered cohesive-frictional soil is highly recommended. The MLP model with $q_{u(c\text{-}\phi)}$ achieved $r = 0.961$ also, and RMSE and MAE values of 3.99 and 3.09, respectively, whilst, for the MLP models with $\tilde{N}_c$ and $\tilde{N}_{c-\phi}$, the values of *r*, RMSE and MAE were found to be 0.942, 5.04 and 3.81, respectively.

Not surprisingly, the weighted-average method (Bowles, 1988) method again performed poorly with a low *r* value of 0.868 and high RMSE and MAE values of 15.71 and 13.14, respectively. In general, the weighted-average method (Bowles, 1988) overestimated the bearing capacity and dangerously so in many cases, as shown in Figure 7.25.

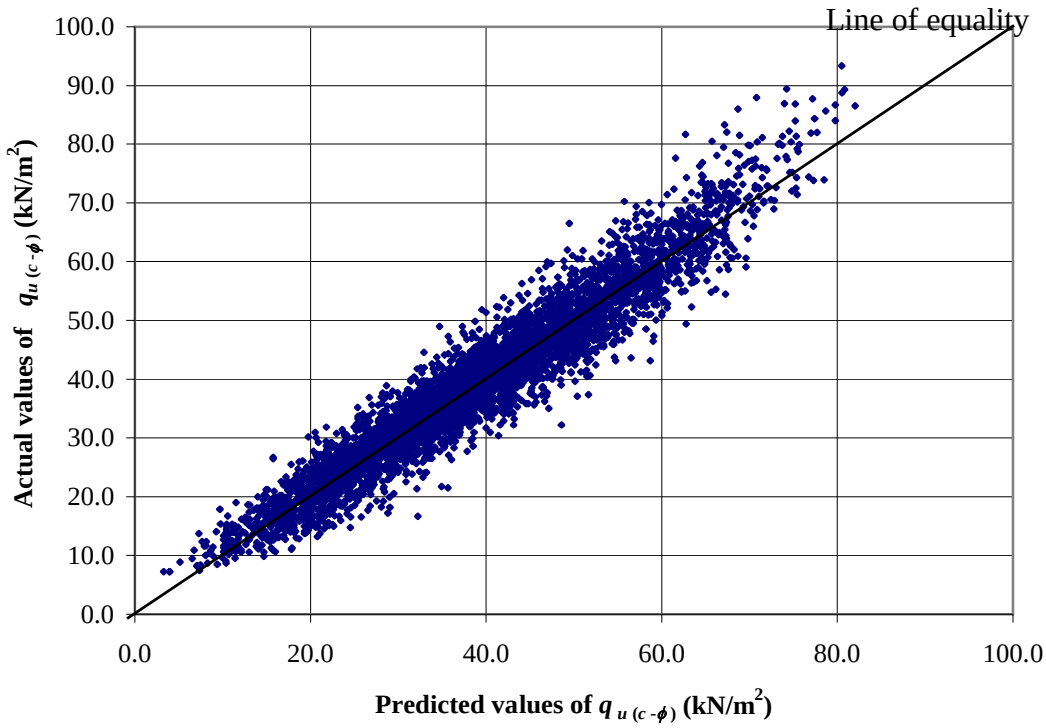


**Figure 7.21** Comparison of actual versus predicted values of bearing capacity using the MLP model for $q_{u(c\text{-}\phi)}$.

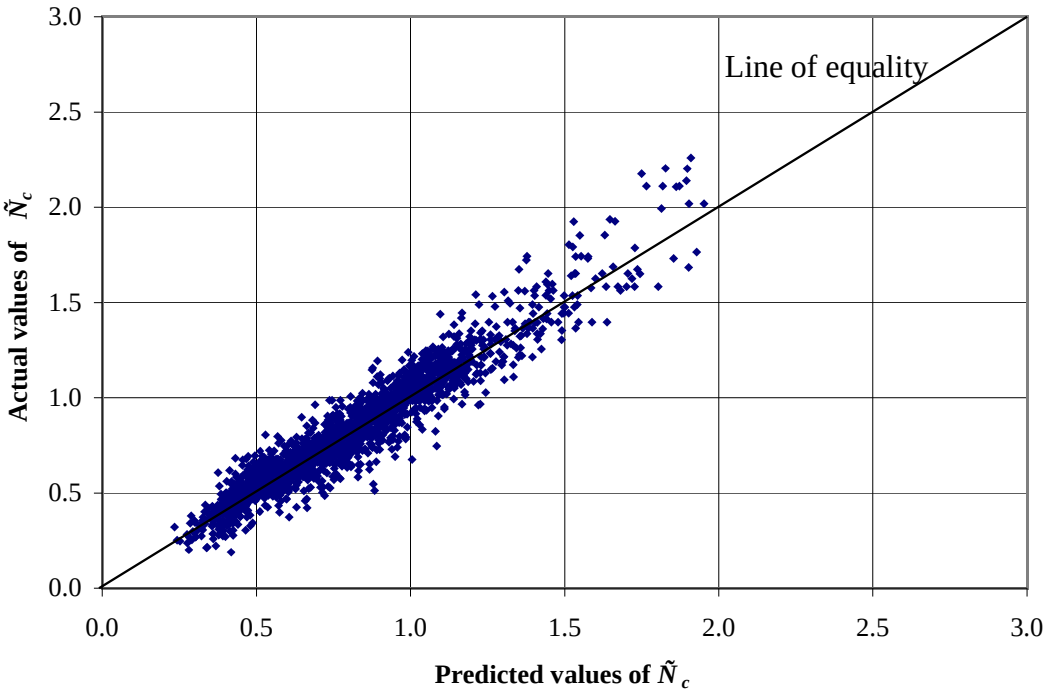


**Figure 7.22** Comparison of actual versus predicted values of $\tilde{N}_c$ using the MLP model with $\tilde{N}_c$.

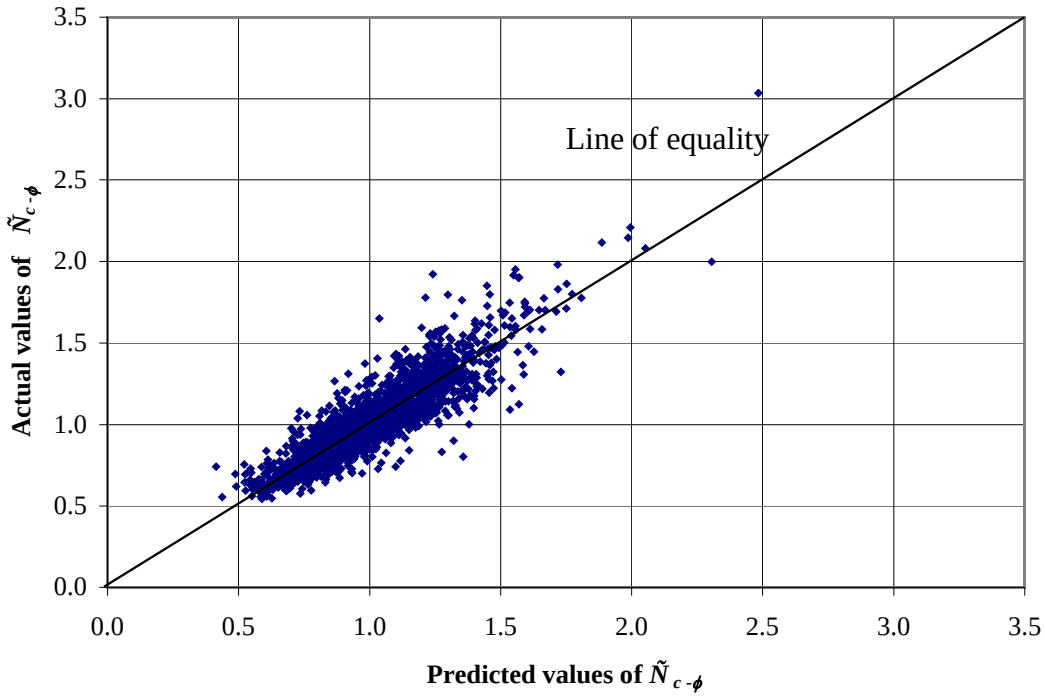


**Figure 7.23** Comparison of actual versus predicted values of $\tilde{N}_{c-\phi}$ using the MLP model with $\tilde{N}_{c-\phi}$.

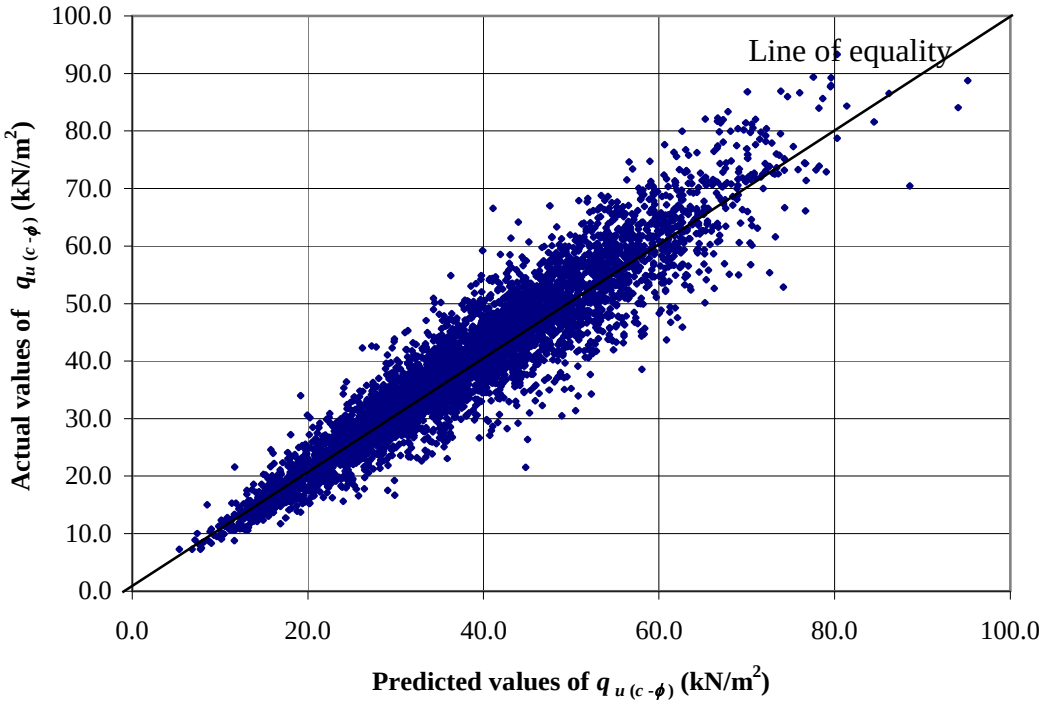


**Figure 7.24** Actual versus predicted values of bearing capacities using the MLP models with $\tilde{N}_c$ and $\tilde{N}_{c-\phi}$.

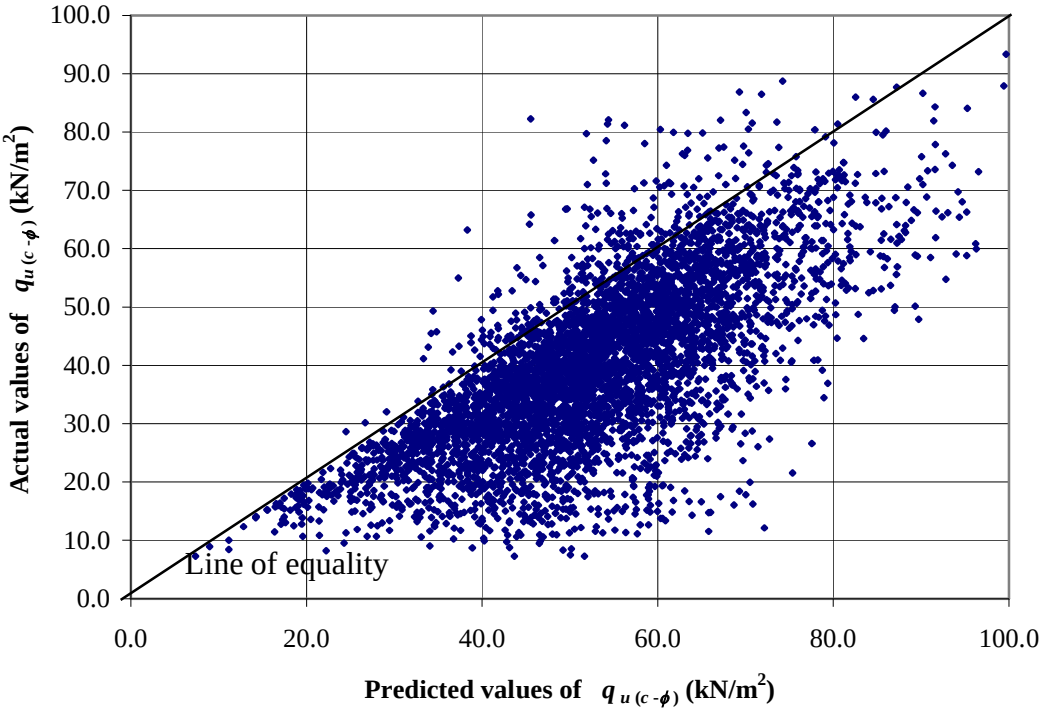


**Figure 7.25** Comparison of the bearing capacities calculated using the weighted-average method (Bowles, 1988) versus actual values for cohesive-frictional soil.

**Table 7.11** Comparison between the MLP models and weighted-average method for bearing capacity prediction for $c$-$\phi$ soil.

| **Performance measurement** | **Methods** | | |
|---|---|---|---|
| | **MLP- $q_{u(c-\phi)}$** | **MLP- $\tilde{N}_c$, $\tilde{N}_{c-\phi}$** | **Weighted-average method (Bowles, 1988)** |
| Correlation coefficient, $r$ | 0.961 | 0.942 | 0.868 |
| RMSE (kN/m$^2$) | 3.99 | 5.04 | 15.71 |
| MAE (kN/m$^2$) | 3.09 | 3.81 | 13.14 |

## 7.8 ILLUSTRATIVE NUMERICAL EXAMPLES

In order to explain better the implementation of the proposed MLP models, multiple illustrative numerical examples are given below.

*Example 1. Purely-cohesive Soil*

A rough footing of width, $B$ = 3.6 m is founded on a 10-layered, purely-cohesive soil with cohesions, $c_i$, and thicknesses, $h_i$, of each of the layers given as follows: $c_{i=1,\ldots,10}$ = {7.86, 5.71, 9.06, 1.67, 2.94, 6.47, 9.08, 1.70, 1.87, 8.67}; $h_{i=1,\ldots,9}$ = {0.2, 1.0, 0.2, 0.8, 0.8, 1.0, 0.2, 0.4, 0.6}. A preliminary estimation of the ultimate bearing capacity of strip footing is required.

*Solution*:

The MLP model for $\tilde{N}_c$ (Equations 7.14 and 7.15) is employed to calculate the ultimate bearing capacity of strip footing, $q_{u(c)}$, as follows:

The values of $c_{i=1,\ldots,10}$, $h_{i=1,\ldots,9}$, and $B$ are substituted into Equation 7.15.

$$T_{i=1,\ldots,9} = \left[1+\exp\left(\begin{array}{l} w_1\times 7.86 + w_2\times 5.71 + w_3\times 9.06 + w_4\times 1.67 + w_5\times 2.94 \\ + w_6\times 6.47 + w_7\times 9.08 + w_8\times 1.70 + w_9\times 1.87 + w_{10}\times 8.67 \\ + w_{11}\times 0.2 + w_{12}\times 1.0 + w_{13}\times 0.2 + w_{14}\times 0.8 + w_{15}\times 0.8 \\ + w_{16}\times 1.0 + w_{17}\times 0.2 + w_{18}\times 0.4 + w_{19}\times 0.6 + w_{20}\times 3.6 + C \end{array}\right)\right]^{-1}$$

By substituting the values of $w_i$ and $C$ given previously in Table 7.5 into the equation above, yields $T_1$ = 0.994; $T_2$ = 0.200; $T_3$ = 0.923; $T_4$ = 0.674; $T_5$ = 0.608; $T_6$ = 0.212; $T_7$ = 0.117; $T_8$ = 0.853; and $T_9$ = 0.985. These values of $T_{i=1,\ldots,9}$ are then substituted into Equation 7.14, which yields:

$$\tilde{N}_c = 2.306\left[1+\exp\left(\begin{array}{l} 6.979\times 0.994 - 2.655\times 0.200 \\ - 2.305\times 0.923 - 2.281\times 0.674 \\ + 1.683\times 0.608 - 1.972\times 0.212 \\ + 4.518\times 0.117 + 3.157\times 0.853 \\ - 2.110\times 0.985 - 2.818 \end{array}\right)\right]^{-1} + 0.174 = 0.54$$

Using Equation 7.8 and setting $\tilde{N}_{c-\phi}$ to be 1.0 for the purely-cohesive case and $N_c$ to be 5.14 (Prandtl's solution), the ultimate bearing capacity of the strip footing, $q_{u(c)}$, is calculated as follows:

$$q_{u\,(c-\phi)} = \tilde{N}_{c-\phi} \times \tilde{N}_c \times N_c \times c_1 = 1.0 \times 0.54 \times 5.14 \times 7.858 = 21.8 \text{ kN/m}^2$$

Hence, the result obtained from MLP model in this example is marginally higher than the result from the numerical finite limit analysis, which is 19.6 kN/m$^2$.

*Example 2. Cohesive-frictional Soil*

A rough footing with a width $B$ = 3.6 m is founded on a 10-layered cohesive-frictional soil with soil cohesions, $c_i$, friction angles, $\phi_i$, and thicknesses, $h_i$, for each of the layers as follows: $c_{i=1,\ldots,10}$ = {7.86, 5.71, 9.06, 1.67, 2.94, 6.47, 9.08, 1.70, 1.87, 8.67}; $\phi_{i=1,\ldots,10}$ = {19.45°, 7.31°, 5.10°, 8.89°, 12.77°, 19.49°, 18.96°, 11.49°, 14.71°, 13.85°}; $h_{i=1,\ldots,9}$ = {0.2, 1.0, 0.2, 0.8, 0.8, 1.0, 0.2, 0.4, 0.6}. Estimate the ultimate bearing capacity of the strip footing.

*Solution*:

Two approaches can be adopted to calculate $q_{u(c\text{-}\phi)}$ as follows:

*Approach 1: Using the MLP model with $q_{u(c\text{-}\phi)}$ (Equations 7.12 and 7.13)*

By substituting the given information of $c_i$, $\phi_i$, $h_i$, and $B$ into Equation 7.13**,** and yields:

$$T_{i=1,\ldots,11} = \left[1 + \exp\left(\begin{array}{l} w_1 \times 7.86 + w_2 \times 5.71 + w_3 \times 9.06 + w_4 \times 1.67 + w_5 \times 2.94 \\ + w_6 \times 6.47 + w_7 \times 9.08 + w_8 \times 1.70 + w_9 \times 1.87 + w_{10} \times 8.67 \\ + w_{11} \times 19.45 + w_{12} \times 7.31 + w_{13} \times 5.10 + w_{14} \times 8.89 \\ + w_{15} \times 12.77 + w_{16} \times 19.49 + w_{17} \times 18.96 + w_{18} \times 11.49 \\ + w_{19} \times 14.71 + w_{20} \times 13.85 + w_{21} \times 0.2 + w_{22} \times 1.0 \\ + w_{23} \times 0.2 + w_{24} \times 0.8 + w_{25} \times 0.8 + w_{26} \times 1.0 \\ + w_{27} \times 0.2 + w_{28} \times 0.4 + w_{29} \times 0.6 + w_{30} \times 3.6 + C \end{array}\right)\right]^{-1}$$

By substituting the values of $w_i$ and $C$ given previously in Table 7.4 into the equation above, yields $T_1$ = 0.956; $T_2$ = 0.974; $T_3$ = 0.016; $T_4$ = 0.617; $T_5$ = 0.954; $T_6$ = 0.222; $T_7$ = 0.658; $T_8$ = 0.154; and $T_9$ = 0.972. The values of $T_{i=1,\ldots,9}$ are then substituted into Equation 7.12 as follows:

$$q_{u(c-\phi)} = 86.065\left[1+\exp\left(\begin{array}{l}4.239\times 0.956 - 3.821\times 0.974\\ +4.867\times 0.016 - 2.804\times 0.617\\ -2.709\times 0.954 - 2.597\times 0.222\\ -3.746\times 0.658 + 3.475\times 0.154\\ +3.613\times 0.972 + 4.080\end{array}\right)\right]^{-1} + 7.245 = 28.0 \text{ kN/m}^2$$

The result obtained from MLP model is slightly lower than that from the numerical finite limit analysis, which is 31.4 kN/m$^2$.

*Approach 2: Using the MLP models with $\tilde{N}_c$ (Equations 7.14 and 7.15) and $\tilde{N}_{c-\phi}$ (Equations 7.16 and 7.17)*

The value of $\tilde{N}_c$ was obtained in the previous solution (i.e. $\tilde{N}_c$ = 0.54). To calculate $\tilde{N}_{c-\phi}$, the given values of $c_i$, $\phi_i$, $h_i$, and $B$ are substituted into Equation 7.17, yielding:

$$T_{i=1,\ldots,9} = \tanh\left(\begin{array}{l}w_1\times 7.86 + w_2\times 5.71 + w_3\times 9.06 + w_4\times 1.67 + w_5\times 2.94\\ +w_6\times 6.47 + w_7\times 9.08 + w_8\times 1.70 + w_9\times 1.87 + w_{10}\times 8.67\\ +w_{11}\times 19.45 + w_{12}\times 7.31 + w_{13}\times 5.10 + w_{14}\times 8.89\\ +w_{15}\times 12.77 + w_{16}\times 19.49 + w_{17}\times 18.96 + w_{18}\times 11.49\\ +w_{19}\times 14.71 + w_{20}\times 13.85 + w_{21}\times 0.2 + w_{22}\times 1.0\\ +w_{23}\times 0.2 + w_{24}\times 0.8 + w_{25}\times 0.8 + w_{26}\times 1.0\\ +w_{27}\times 0.2 + w_{28}\times 0.4 + w_{29}\times 0.6 + w_{30}\times 3.6 + C\end{array}\right)$$

By substituting the values of $w_i$ and $C$ given previously in Table 7.6 into the equation above, yields $T_1$ = 0.297; $T_2$ = -0.754; $T_3$ = -0.230; $T_4$ = -0.996; $T_5$ = 0.193; $T_6$ = 0.310; $T_7$ = 0.475; $T_8$ = 0.666; and $T_9$ = -0.629. The values of $T_{i=1,\ldots,9}$ are then substituted into Equation 7.16 to obtain $\tilde{N}_{c-\phi}$ as follows:

$$\tilde{N}_{c-\phi} = 2.511\left[1+\exp\begin{pmatrix}1.432\times 0.297-1.254\times(-0.754)\\+0.789\times(-0.230)-1.952\times(-0.996)\\+0.898\times 0.193-1.009\times 0.310\\+0.289\times 0.475-1.017\times 0.666\\+0.593\times(-0.629)-0.335\end{pmatrix}\right]^{-1}+0.524=0.67$$

By using Equation 7.8, the ultimate bearing capacity of strip footing, $q_{u(c)}$, is calculated as follows:

$$q_{u\,(c-\phi)} = \tilde{N}_{c-\phi}\times\tilde{N}_{c}\times N_{c}\times c_1 = 0.65\times 0.54\times 14.33\times 7.86 = 39.53\ \text{kN/m}^2$$

where $N_c$ is calculated using Equation 7.9 by substituting $\phi_1 = 19.45°$ as follows:

$$N_c = \frac{e^{\pi\tan\phi_1}\tan^2\left(\frac{\pi}{4}+\frac{\phi_1}{2}\right)-1}{\tan\phi_1} = 14.33$$

The result given by the equation above is 25% higher than the result from numerical finite limit analysis, which is 31.4 kN/m$^2$.

## 7.9 SUMMARY AND CONCLUSIONS

This chapter described the development of meta-models for predicting the bearing capacity of footings on multi-layered, cohesive-frictional, weightless soil. Two numerical models were used, namely, the finite element lower bound analysis and the artificial neural network (ANN) technique. A total of 5,000 Monte Carlo realisations were carried out using the finite element lower bound analyses, and the results of these analyses were used in training, validating and testing sets of multi-layer perception (MLP) models

New design equations were derived based on the developed optimal MLP models; that is, those based on: $q_{u(c\text{-}\phi)}$ in Equations 7.12 and 7.13; $\tilde{N}_c$ in Equations 7.14 and 7.15; and $\tilde{N}_{c-\phi}$ in Equations 7.16 and 7.17. Sensitivity analyses were also carried out

to test the robustness of the MLP models with respect to the various parameters influencing the models.

The predictions from the MLP models and weighed average method (e.g. Bowles 1988) method were compared and the results discussed. The results indicated that the MLP models outperformed the weighted average method and are able to predict bearing capacities reliably and relatively accurately, and consequently, their use in practice is encouraged. The performances of each of the models did not differ significantly from one another, although, the MLP model based on $q_{u(c\text{-}\phi)}$ in Equations 7.12 and 7.13 slightly outperformed the MLP model based on $\tilde{N}_c$ and $\tilde{N}_{c-\phi}$ in Equations 7.14 to 7.17 in cohesive-frictional cases. The MLP model based on $\tilde{N}_c$ and $\tilde{N}_{c-\phi}$ in Equations 7.14 to 7.17 clearly outperformed the MLP model developed in Chapter 6 for purely cohesive cases.

There are a number of important limitations. For example, the lower bound computations were carried out under plane-strain conditions implying the models are valid solely for strip footings. It would be possible to develop ANN-based models for rectangular footings, or circular footings, if three-dimensional finite element limit analysis was adopted, with the length or diameter as an additional parameter. Another limitation in this study is the range of variables employed in ANN training, which ultimately limits the applicability of MLP models, since the ANNs should be used only for interpolation. Finally, it can be seen that, although large number of Monte Carlo simulations were carried out, not all possible cases were analysed and included in ANN training, thus diminishing the predictability of ANN-based models.

# CHAPTER 8

## SUMMARY AND CONCLUSIONS

## 8.1 SUMMARY

This study quantified the effects of soil variability on a strip footing placed on single- and two-layered spatially variable purely cohesive soils. In addition, meta-models were developed, which are useful for making preliminary estimates of the bearing capacity of footings on multi-layered, purely cohesive and cohesive-frictional soils profiles. This study, however, focused on the cohesive term, $N_c$, of Terzaghi's bearing capacity equation by assuming weightless soil and in the absence of surcharge, and therefore, both $N_q$ and $N_\gamma$ were omitted.

In Chapter 2, previous research into the bearing capacity of footings on multi-layered and spatially random soils has been presented, with an emphasis on the analysis of shallow strip footings. It was shown that some research has been undertaken in the past on non-homogeneous and layered soil profiles and the use of the rigorous solutions obtained from these studies in practical design is highly recommended. Finally, it was observed that little progress has been made in predicting the ultimate bearing capacity of footings founded on multiple layers of soil using relatively simple hand calculation methods.

The methodologies adopted in this study to quantify the effects of soil variability on the bearing capacity of shallow strip footings were described. The methods adopted include numerical methods to determine the ultimate bearing capacity and load-settlement responses of foundations and local average subdivision (LAS) to simulate spatially variable soils. Artificial neural networks (ANNs) were used to develop meta-models for bearing capacity prediction. The upper and lower bound limit analyses were based on the plastic limit theorem and their numerical implementations were used to calculate the collapse load. The feature of bracketing the solution provides a built-in error check on the accuracy of the computed collapse load. A brief discussion of the traditional displacement finite element analysis was also presented in Chapter 3. Furthermore, a discussion of local average subdivision (LAS), which is based on random field theory, was also given. The structure and operation of ANNs, as well as the development of ANN models were also described. ANNs learn by being presented with training data from which the ANN network adjusts weights to find a set of weights that produce the optimum input/output data mappings. Many

factors that affect the development of ANN models were addressed. These include the determination of model inputs, division of data, data pre-processing, determination of model architecture, model optimisation, stopping criteria and model validation.

In Chapter 4, the numerical modelling of strip footings founded under plane strain conditions was presented. This was carried out for 2-layered profiles, namely, purely cohesive and cohesive-frictional materials. The results obtained from the numerical methods were examined to ensure that the results were both accurate and robust. In the latter part of this thesis, the robustness of the random field generation using LAS was examined to ensure and confirm that the simulated profiles conformed to the target statistical distribution and underlying correlation structure.

In Chapter 5, the results of analyses on the effects of spatially random soil on the bearing capacity of strip footings founded on single- and two-layered purely cohesive soils were presented. Under this investigation, Monte Carlo simulations with 500 realisations were used and the local average subdivision (LAS) method was implemented into both the lower and upper bound finite element methods. The random soil profiles are simulated using LAS method over a range of soil variability and scales of fluctuation, i.e. $COV_c$ and $\theta_c$. Modified bearing capacity factors, $N^*_c$, were then acquired using both the lower and upper bound finite element methods. The average and coefficient of variation (*COV*) of the bearing capacity factors over 500 realisations, i.e. $\mu_{N^*c\,\mathrm{AV}}$ and $COV_{N^*c\,\mathrm{AV}}$, were used to quantify the effects of soil variability on the bearing capacity. The variations of these two parameters with respect to soil variability and scales of fluctuation were then analysed and some useful conclusions were derived. These include:

- The mean of $N^*_c$, $\mu_{N^*c}$, decreases in both single- and two-layered cohesive deposits as the soil variability increases.

- The greatest reduction of $\mu_{N^*c}$ was observed when $\theta_c \approx 0.5B$ and $COV_c$ = 100% for the single-layered case. It was shown that the value of $\mu_{N^*c}$ is 38% below the deterministic solution.

- In the single-layered case, when the scales of fluctuation are either extremely small or infinitely large, the value of $\mu_{N^*c}$ should revert to the deterministic solution.

- In two-layered cases, when a weak layer is underlain by a strong layer and $H/B$= 0.25 to 0.5, the worst-case scenario occurred when $\theta_c \approx 0.1B$ or less and $COV_c$ = 100%. However, when $H = 1.0B$, the greatest reduction of $\mu_{N^*c}$ occurred when $\theta_c \approx 0.25B$ and $COV_c$ = 100%. The $\mu_{N^*c\ \mathrm{AV}}$ are 29% - 38% less than the deterministic value in worst-case scenarios for different $H/B$ ratio.

- When the footing is founded on a strong layer and underlain by a weaker layer, the worst-case scenario occurs when $0.5B \leq \theta_c \leq 1.0B$ and $COV_c$ = 100% for all $H/B$ ratios. The reduction of $\mu_{N^*c\ \mathrm{AV}}$ value for the worst-case scenario is around 37% less than deterministic value.

- In the two-layered case, as $H/B$ increases, the variations of $\mu_{N^*\mathrm{c\ AV}}$ and $COV_{N^*c\ \mathrm{AV}}$ with respect to soil variability and scales of fluctuation are similar to those obtained in the single-layered case.

- For the two-layered cases, theoretically, the $\mu_{N^*c}$ will revert to the deterministic solution as $\theta_c \rightarrow 0$. However, as $\theta_c \rightarrow \infty$ and $COV_c$ is very high, it has been demonstrated that there were large proportions of realizations where the ratio of $\mu_{c1} / \mu_{c2}$ falls outside the intended study ranges under these circumstances. As a consequence, $\mu_{N^*c}$ will not revert to deterministic solution, and thus the accuracy of $COV_{N^*c\ \mathrm{AV}}$ is also affected.

- In addition, the coefficient of variation of the bearing capacity factor, $COV_{N^*c}$, was found to be positively correlated with both soil variability and scales of fluctuation in both the single- and two-layered cases. When the normalised parameter $COV_{N^*c}/COV_c$ was used, it was clearly shown that the $COV_{N^*c}/COV_c$ does not vary with $COV_c$, but with the $\theta_c/B$.

- By examining the upper bound failure mechanism, it was found that the inherent spatial variability of soil shear strength alters the failure mechanism from a symmetrical log spiral mechanism in homogeneous soil cases to a non-symmetrical mechanism, particularly when the variability of soil properties is high.

Chapter 6 described two multi-layer perceptrons (MLP) models developed to provide a reliable and robust estimation of bearing capacity of footings on four- and ten-layered purely-cohesive soil. This chapter detailed the methodologies used in developing the optimum model, including the data generation using Monte-Carlo simulation and the development of the ANN-based models. This chapter also presented a comparison between the results obtained using the ANN-based models and the weighted average method (Bowles 1988). The analyses carried out in this chapter yielded the following conclusions:

- The optimum model for the four-layered cohesive soil developed in this work was obtained using one hidden layer with five hidden layer nodes, the sigmoid transfer function in both the hidden and output layers, a momentum term of 0.8 and a learning rate of 0.2.

- Whilst the optimum model for ten-layered cohesive soil was obtained using one hidden layer with seven hidden layer nodes, the sigmoid transfer function in both the hidden and output layers, a momentum term of 0.8 and a learning rate of 0.2.

- The results of the sensitivity analysis indicated that the footing width, the cohesions and the thicknesses of the uppermost layers have the most significant impact on the bearing capacity of the shallow strip footing. On the other hand, the impact of the cohesion and thickness of the subsequent layers on the bearing capacity of the shallow strip footing reduces as they are further away from the footing.

- The results indicated that the MLP models are able to predict well the bearing capacity of a strip footing founded on multi-layered purely cohesive soils and significantly outperformed other methods. The sensitivity analysis carried out to test the robustness of the developed MLP model, and consequently the ANN-based design equation, indicated that the model is robust and can be used for predictive purposes with confidence.

- However, both upper and lower bound computations were carried out in 2-dimensions and it was assumed that the footing has infinite length in the out-of-plane direction. It would be desirable to vary the length of a rectangular footing in the future so that the upgraded model can accurately predict the bearing capacity of three-dimensional pad footings.

Finally, in Chapter 7, the objectives were to develop meta-models for predicting the bearing capacity of strip, rough footings supported on a ten-layered, cohesive-frictional, homogeneous and weightless material. The details of two proposed methodologies for developing two meta-models were presented. The feasibility of utilising the ANNs technique for predicting the bearing capacity of shallow strip footing on multi-layered soils has been assessed using MLPs trained with the back-propagation algorithm. In order to test the robustness of the developed MLP, a sensitivity analysis on each of the influencing factors was carried out. Three new tractable design equations based on the MLP models, were derived to facilitate the use of the model. The predictions from the ANN-based models and the other methods were compared. The results and conclusions of this work are as follows:

- The optimum models for both $q_{u(c\text{-}\phi)}$ and $\widetilde{N}_c$ were obtained using 1 hidden layer with 9 hidden layer nodes, the sigmoid transfer functions in both the hidden and output layers, a momentum term of 0.8 and a learning rate of 0.2.

- The optimum model for $\widetilde{N}_{c-\phi}$ was obtained using 1 hidden layer with 9 hidden layer nodes, the tanh transfer function in the hidden layer, the sigmoid transfer function in the output layer, a momentum term of 0.8 and a learning rate of 0.2.

- The results of this work indicate that the MLP models are able to predict well the bearing capacity of a strip footing on cohesive-frictional multilayered soils and significantly outperformed the weighted average method. The sensitivity analysis carried out to test the robustness of the developed MLP model, and consequently the MLP-based design equation, indicated that the model is robust and can be used for predictive purposes with confidence.

- The MLP model based on $q_{u(c\text{-}\phi)}$ in Equations 7.12 and 7.13 slightly outperformed the MLP model based on $\tilde{N}_c$ and $\tilde{N}_{c-\phi}$ in Equations 7.14 to 7.17 in the cohesive-frictional cases. The predictions from MLP model, based on $\tilde{N}_c$ and $\tilde{N}_{c-\phi}$ in Equations 7.14 to 7.17, clearly outperformed the MLP model developed in Chapter 6 for purely cohesive soil.

- As in the previous chapters, two-dimensional footing analyses were performed, and as a result, these models are valid solely for strip footings.

## 8.2 RECOMMENDED FURTHER RESEARCH

Because very little work has been done on examining the bearing capacity of footings on spatially random soil profiles, and this study is certainly the first using finite element upper and lower bound methods to study the effect of soil variability on the bearing capacity of strip footings, this study has dealt with the relatively simple cases of dealing with single and two-layered purely cohesive soil profiles. This study employed the idealisation of weightless soil, and therefore only focused on the cohesive term, $N_c$, of the bearing capacity equation. Both the $N_q$ and $N_\gamma$ terms were omitted. Natural soil has unit weight, $\gamma$, so it should be included in future research. To implement the bulk unit weight in finite element analyses, it is recommended that the void ratio, $e$, might first be determined or specified, as the void ratio is one of the fundamental soil parameters. The bulk unit weight of soil can then be calculated using phase relationships.

Due to the constraints on available resources (e.g. length of PhD candidature and computing resources) adopted in this study, several simplifications and assumptions

have been made in the study of the effect of soil variability, Chapter 5, to achieve manageable computation effort and, at the same time, maintaining reasonable accuracy of results. As a result, the number of parameters examined was limited. Some of the variables, which were not included in this study, may impact on the results and could be considered in the future research. Examples of these variables include:

- Smooth and rough footings (with varying roughness coefficients);
- Multiple footings;
- More complex multi-layered soil profiles;
- Anisotropic correlation structures; and
- Various combinations of cohesive-frictional material and purely frictional material.

Furthermore, 2-dimensional (2-D) finite element analyses were used in this study, which implies that all the numerical studies were conducted under plane strain conditions. This implies that the results obtained from the analyses are applicable only to strip footings. As computer-processing power increases in the future and further progress is made in the area of numerical analysis, the use of 3-D finite element analysis will become more efficient technique for simulating circular, square and rectangular shaped footings. Furthermore, analysing footings on purely frictional materials required that high concentrations of elements be placed in areas where high stress gradients or high velocity gradients are likely to occur; that are at the edges of the footings. In order to employ a fan type mesh suggested by Shiau et al. (2003) and discussed in Chapter 4, some modifications on to the LAS implementation are required to allow irregular elements shapes, which in this stage only allows regular rectangular elements.

This study has demonstrated that ANNs have the ability to predict the bearing capacity of shallow foundations on purely cohesive and cohesive-frictional soil. However, Rezania and Javadi (2007) have recently presented a new genetic programming (GP) based model for predicting the settlement of shallow foundations. They showed that, like ANN, the GP model is capable of rendering the complex

relationship between foundation settlement and its contributing factors in the form of a very straightforward mathematical function. The GP model clearly outperformed the traditional methods, and also slightly improved upon the predictions given by the ANN models suggested by Shahin et al. (2002) and described in Chapter 3. Furthermore, the GP generates a simple and lean structured representation of the system. It is a promising approach to provide more tractable and slightly superior models to those presented in this study. The GP model will likely to gain momentum in the future research. Therefore, it is recommended that GP models be explored in future research. These include models, which incorporate $N_c$, $N_q$, and $N_\gamma$.

## 8.3 CONCLUSIONS

From the analyses presented in this thesis, it can be concluded that the mean of $N^*_c$, $\mu_{N^*c}$, decreases in both single- and two-layered cohesive soil profiles as the soil variability increases. The worst-case scenarios for both the single- and two-layered cases are when the scales of fluctuation are smaller than footing width. Moreover, the coefficient of variation of the modified bearing capacity factor, $COV_{N^*c}$, was found to be positively correlated with both the variability of soil and scales of fluctuation in both single- and two-layered cases.

In addition, it has been demonstrated that the artificial neural networks (ANNs) have the ability to accurately predict the bearing capacity of shallow strip footing founded on multi-layered purely-cohesive and cohesive-frictional weightless materials. Furthermore, the MLP models that were developed in this work can be translated into relative simple equations suitable for hand calculations, which allow practitioners to relatively easily predict the bearing capacity of footings on multi-layered soil.